BIOCHEMISTRY
including biophysical chemistry & molecular biology
Article

Biochemistry **2010,** *49,* 10421–10439 10421
DOI: 10.1021/bi1012518

Characterization of Nicotinamidases: Steady State Kinetic Parameters, Classwide Inhibition by Nicotinaldehydes, and Catalytic Mechanism†

Jarrod B. French,[‡,§] Yana Cen,[∥] Tracy L. Vrablik,[⊥] Ping Xu,[∥] Eleanor Allen,[∥] Wendy Hanna-Rose,[⊥] and Anthony A. Sauve*[,∥]

[‡]*Department of Chemistry and Chemical Biology, Cornell University, Ithaca, New York 14853, United States,* [§]*Tri-Institutional Program in Chemical Biology, Cornell University, 1300 York Avenue, New York, New York 10065, United States,* [∥]*Department of Pharmacology, Weill Medical College of Cornell University, 1300 York Avenue, New York, New York 10065, United States, and* [⊥]*Department of Biochemistry and Molecular Biology, The Pennsylvania State University, University Park, Pennsylvania 16802, United States*

Received August 5, 2010; Revised Manuscript Received October 24, 2010

ABSTRACT: Nicotinamidases are metabolic enzymes that hydrolyze nicotinamide to nicotinic acid. These enzymes are widely distributed across biology, with examples found encoded in the genomes of Mycobacteria, Archaea, Eubacteria, Protozoa, yeast, and invertebrates, but there are none found in mammals. Although recent structural work has improved our understanding of these enzymes, their catalytic mechanism is still not well understood. Recent data show that nicotinamidases are required for the growth and virulence of several pathogenic microbes. The enzymes of *Saccharomyces cerevisiae*, *Drosophila melanogaster*, and *Caenorhabditis elegans* regulate life span in their respective organisms, consistent with proposed roles in the regulation of NAD^+ metabolism and organismal aging. In this work, the steady state kinetic parameters of nicotinamidase enzymes from *C. elegans*, *Sa. cerevisiae*, *Streptococcus pneumoniae* (a pathogen responsible for human pneumonia), *Borrelia burgdorferi* (the pathogen that causes Lyme disease), and *Plasmodium falciparum* (responsible for most human malaria) are reported. Nicotinamidases are generally efficient catalysts with steady state k_{cat} values typically exceeding 1 s^{-1}. The K_m values for nicotinamide are low and in the range of 2−110 μM. Nicotinaldehyde was determined to be a potent competitive inhibitor of these enzymes, binding in the low micromolar to low nanomolar range for all nicotinamidases tested. A variety of nicotinaldehyde derivatives were synthesized and evaluated as inhibitors in kinetic assays. Inhibitions are consistent with reaction of the universally conserved catalytic Cys on each enzyme with the aldehyde carbonyl carbon to form a thiohemiacetal complex that is stabilized by a conserved oxyanion hole. The *S. pneumoniae* nicotinamidase can catalyze exchange of ^{18}O into the carboxy oxygens of nicotinic acid with $H_2{}^{18}O$. The collected data, along with kinetic analysis of several mutants, allowed us to propose a catalytic mechanism that explains nicotinamidase and nicotinic acid ^{18}O exchange chemistry for the *S. pneumoniae* enzyme involving key catalytic residues, a catalytic transition metal ion, and the intermediacy of a thioester intermediate.

The nicotinamidases hydrolyze nicotinamide to nicotinic acid (Scheme 1). They play important roles in nicotinamide salvage in multiple species of bacteria (*1*), mycobacteria (*1*−*4*), yeast (*5*−*7*), and protozoa (*8*) and are encoded in genomes of plants (*9*) and in many metazoan species, such as *Drosophila melanogaster* (*10*) and *Caenorhabditis elegans* (*10*−*12*). Nicotinamide salvage is important because $NAD(P)^{+1}$ is chemically unstable to non-enzymatic hydrolysis even at physiologic temperatures (*13*−*15*) and nicotinamide is the product of multiple NAD^+-consuming enzymes (*13*, *14*), such as sirtuins, that are widely distributed in biology (*16*). Consistent with their centrality to NAD^+ homeostasis, nicotinamidases have been shown to be essential for the viability of several microorganisms that are pathogenic to humans such as *Borrelia burgdorferi* (which causes Lyme disease) (*17*−*19*) and *Brucella abortus* (*20*). It is possible that other pathogenic organisms require this enzyme as well, because some of these, including *Plasmodium falciparum,* do not appear to encode genes for enzymatic components of de novo NAD^+ biosynthetic pathways (*21*). Consequently, it is likely that these organisms are highly reliant on salvage of nicotinamide from the human host. Attractively, human and mammalian genomes do not encode a nicotinamidase, suggesting that small molecule inhibitors of nicotinamidases could serve as antimicrobial agents (*21*).

Biologically interesting roles for nicotinamidases have also been identified as increasers of life span in *D. melanogaster* (*10*)

†This work was funded by the Tri-Institutional Program in Chemical Biology of Cornell University and by the Milstein Institute for Chemical Biology of the Weill Medical College of Cornell University. The work was also funded by the NIH, R01 DK74366-01 (A.A.S) and R01-GM086786 (W.H.-R.).

*To whom correspondence should be addressed: Department of Pharmacology, Weill Medical College of Cornell University, New York, NY 10065. Telephone: (212) 746-6224. Fax: (212) 746-8835. E-mail: aas2004@med.cornell.edu.

[1]Abbreviations: AbPncA, *Acinetobacter baumanii* nicotinamidase; BbNic, *Borrelia burgdorferi* nicotinamidase; cADPR, cyclic ADP-ribose; CePNC1, *Caenorhabditis elegans* nicotinamidase 1; CePNC2, *C. elegans* nicotinamidase 2; DTT, dithiothreitol; GDH, glutamate dehydrogenase; HR-MS, high-resolution mass spectometry; IPTG, isopropyl β-D-1-thiogalactopyranoside; MALDI-TOF, matrix-assisted laser desorption ionization time-of-flight; NA, nicotinic acid; NAD^+, nicotinamide adenine dinucleotide; NADH, nicotinamide adenine dinucleotide, reduced form; NAM, nicotinamide; $NADP^+$, nicotinamide adenine dinucleotide phosphate; NADPH, nicotinamide adenine dinucleotide phosphate, reduced form; NMN, nicotinamide mononucleotide; NR, nicotinamide riboside; PDB, Protein Data Bank; PfNic, *Plasmodium falciparum* nicotinamidase; Pnc1, *Saccharomyces cerevisiae* nicotinamidase; PncA, *Mycobacterium tuberculosis* nicotinamidase; SpNic, *Streptococcus pneumoniae* nicotinamidase.

© 2010 American Chemical Society
Published on Web 10/27/2010

Scheme 1: Nicotinamidase Hydrolyzes Nicotinamide To Form Nicotinic Acid

Scheme 2: Nicotinamidase Catalyzes the Conversion of Pyrazinamide to Pyrazinoic Acid

and *C. elegans* (*11*) and in the budding yeast *Saccharomyces cerevisiae* (*22*). Specifically, nicotinamidases regulate intracellular nicotinamide concentrations, which are implicated in negative regulation of NAD^+-dependent deacetylases (the sirtuins) (*16*, *23*). Overexpression of nicotinamidases increases life span and requires sirtuin activity in yeast (*24*) and in flies (*10*), consistent with the idea that nicotinamidase overexpression depletes intracellular nicotinamide concentrations, thereby increasing sirtuin activity. Consistently, sirtuin overexpression within *D. melanogaster* (*25*, *26*), *C. elegans* (*27*, *28*), and *Sa. cerevisiae* (*29*, *30*) also increases life span. Stresses that increase lifespan in *Sa. cerevisiae*, such as low calorie stress, are inducers of nicotinamidase transcription and translation (*22*), and oxidative stress increases the level of nicotinamidase expression in *D. melanogaster* (*10*). These data suggest that these enzymes are central to phylogenetically conserved adaptive responses to environmental stresses in single-celled eukaryotes and in nonmammalian multicellular eukaryotes. Of additional interest, the nicotinamidase from *Mycobacterium tuberculosis* is responsible for activation of the prodrug pyrazinamide to the active antibiotic pyrazinoic acid. Mutations in this enzyme are associated with resistance to the drug (Scheme 2) (*4*). Recently, nicotinamidases have been shown to be important for plant germination as well (*31*). The available literature supports the view that nicotinamidases are therapeutically and biologically interesting enzymes with diverse functions associated with their enzymatic activity.

The first nicotinamidase activity was reported for the organism *Lactobacillus arabinosus* (*32*), but decades later, there is still limited insight into the chemical and enzymatic mechanisms of these enzymes. Two unliganded structures of nicotinamidases have been reported, one for the *Sa. cerevisiae* enzyme (*6*) and the other from the archaean thermophile *Pyrococcus horikoshii* (*33*). Both structures revealed an active site-coordinated metal ion, proposed to be Zn^{2+}, and similar structural folds, although limited insight into catalytic chemistry was provided. A recent structure of the nicotinamidase from *Acinetobacter baumanii* in complex with nicotinic acid clarified some aspects of the active site design for these enzymes (*34*). The crystal structure revealed that the pyridine N1 atom of nicotinic acid is coordinated to the central metal ion, suggesting that coordination of nicotinamide to the metal center organizes the pyridine for attack by a cysteine residue on the amide carbonyl of the substrate (*34*). This cysteine is universally conserved in all nicotinamidases (Figure 1) and previously had been proposed to perform a nucleophilic function on the enzyme to form a labile thioester of nicotinic acid, which can further hydrolyze to release the free thiol and nicotinic acid (*33*, *34*). This mechanistic proposal was more convincingly demonstrated in a very recent paper, to which several of the current authors contributed, which structurally characterized the thioester intermediate on the nicotinamidase from *Streptococcus pneumoniae* (*35*).

In this paper, we characterize the steady state kinetic properties of nicotinamidases from multiple sources (*Sa. cerevisiae*, *B. burgdorferi*, *Pl. falciparum*, and *S. pneumoniae*) and two nicotinamidase isoforms from *C. elegans*. We present a continuous assay for monitoring nicotinamidase catalytic function and show that these enzymes have high catalytic efficiencies for nicotinamide and can accept a number of additional substituted nicotinamide substrates. The nicotinamidase from *S. pneumoniae* is shown to exchange ^{18}O into nicotinic acid from $H_2{}^{18}O$. In addition, we found that all of these enzymes are inhibited by nicotinaldehyde with K_i values between 1.4 μM and 11 nM. Kinetic analyses revealed that nicotinaldehyde is a competitive inhibitor with nicotinamide, consistent with reversible mechanism-based trapping of the enzyme. Structural variants of nicotinaldehyde were synthesized and biochemically evaluated, establishing the possibility of developing potent yet selective inhibitors for nicotinamidases derived from different sources. Using information provided by nicotinaldehyde inhibition studies, kinetic studies, sequence comparisons, and mutagenesis data, we present mechanisms of nicotinaldehyde inhibition, ^{18}O exchange, and nicotinamide hydrolysis catalyzed by nicotinamidases.

MATERIALS AND METHODS

Reagents and Instrumentation. Unless otherwise stated in the text, all reagents were purchased from Sigma-Aldrich or VWR and were of the highest purity commercially available. UV analyses were performed on a Hitachi U-3010 spectrophotometer. Fluorescence analyses were performed on a LJL Biosystems Analyst AD 96.384 microplate reader.

Plasmid Construction and Protein Expression. Standard molecular biology techniques were used to clone the genes of interest. The cloning and expression of nicotinamidases from *S. pneumoniae*, *B. burgdorferi*, and *Pl. falciparum* (SpNic, BbNic, and PfNic, respectively) are reported in the Supporting Information. The nicotinamidase gene from *B. burgdorferi* was cloned from a pBBE22 construct provided by S. J. Norris (University of Texas Health Science Center, Houston, TX) (*36*). *C. elegans* Pnc1 and Pnc2 (CePNC1 and CePNC2, respectively) were expressed and purified as described previously (*12*), and the expression plasmid of *Sa. cerevisiae* Pnc1 was received as a gift from J. Smith of the University of Virginia (Charlottesville, VA) and expressed and purified as described previously (*24*). Mutants of nicotinamidase from *S. pneumoniae*, R97A, K103A, C136A, and C136S, were prepared in a manner consistent with instructions of the QuickChange site-directed mutagenesis kit (Agilent Technologies, Genomics), and each mutant was confirmed by sequencing. Primers for the mutagenesis are reported in the Supporting Information. Mutants were expressed in the same manner as native SpNic. Proper folding of mutant enzymes was confirmed by native gel electrophoresis. For all of the experiments that follow, the enzyme concentrations were determined by the method of Bradford (*37*).

GDH-Coupled Nicotinamidase Assay. Nicotinamidase activity was monitored by coupling the production of ammonia with the consumption of NAD(P)H by the enzyme bovine glutamate dehydrogenase (GDH, from Sigma). A typical reaction

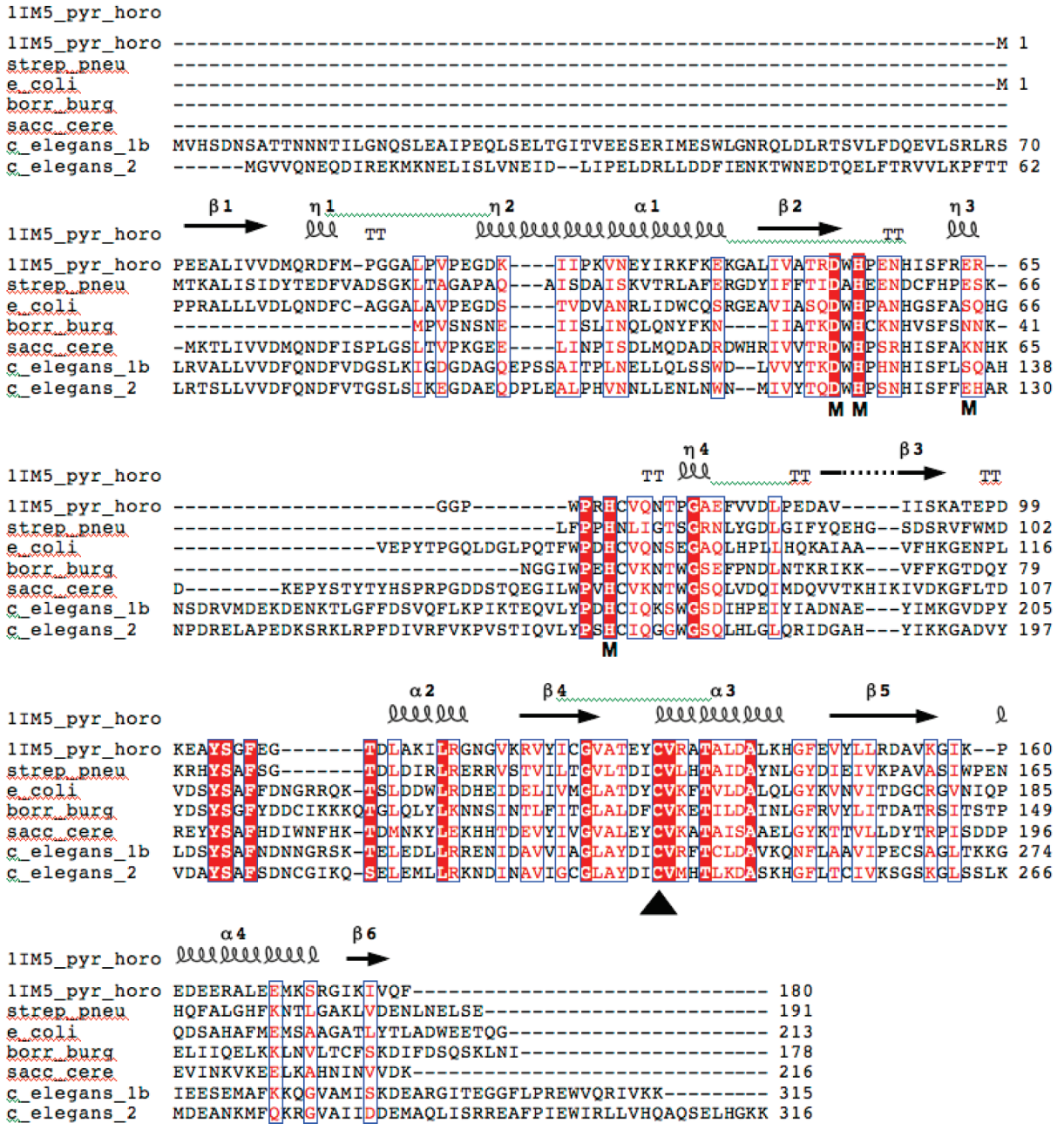

FIGURE 1: Multiple-sequence alignment of the *P. horikoshii* (PDB entry 1IM5), *S. pneumoniae*, *Escherichia coli*, *Sa. cerevisiae*, and *B. burgdorferi* nicotinamidases. The alignment was performed with ClustalW (*56*) and edited with ESPript (*57*). Identical residues are highlighted, and the secondary structure elements of the determined *P. horikoshii* structure (*33*) are shown above the alignment. Vertical arrows point to the proposed catalytic triad proposed by Du et al. that is composed of an aspartate, a cysteine, and a lysine. The proposed metal-binding residues are shown with an M under the appropriate residue.

mixture contained 1 mM α-ketoglutarate, 250 μM NAD(P)H, 1.5 units of GDH per 100 μL of reaction volume, and different concentrations of nicotinamide in 100 mM phosphate buffer (pH 7.3) at 25 °C. The components were mixed and placed in cuvettes (for analysis by UV, 340 nm detection wavelength) or into a 96-well plate (for analysis on a plate reader using fluorescence). Reaction was initiated by addition of the appropriate nicotinamidase enzyme. Typical enzyme concentrations were as follows: 140 nM BbNic, 14 nM PfNic, 210 nM Pnc1, 12 nM SpNic, 10 nM CePNC1, and 133 nM CePNC2. The absorbance at 340 nm was used to monitor the concentration of NAD(P)H with time. In plate reader experiments, the fluorescence intensity was used to monitor NADP(H) (excitation at 360 nm, and emission at 490 nm).

High-Performance Liquid Chromatography (HPLC) Assay for Nicotinamidase Activity. All HPLC analyses were performed on a Hitachi Elite Lachrom system equipped with a diode array detector. After a typical injection on a Macherey-Nagel Nucleosil C-18 250 mm × 4.6 mm column, the mixture was eluted with 20 mM ammonium acetate (pH 6.9) at 1 mL/min for 15 min and then eluted with 20 mM ammonium acetate (pH 6.9) and 10% methanol. Authentic nicotinic acid eluted at 4.2 min and nicotinamide at 16 min using 260 nm as a detection wavelength (typical chromatograms are available in the Supporting Information). In some instances, a Waters 300 mm × 7.8 mm Delta-pak C18 column was used for HPLC measurements with slight adjustments to the assay method. A typical reaction was conducted in a 50 μL total volume containing 200 μM nicotinamide

in 100 mM phosphate buffer (pH 7.3). Reaction was initiated by addition of nicotinamidase (final concentration of 10−200 nM) and the mixture incubated for 20 min at 25 °C. Reactions were quenched by addition of 6 μL of 10% trifluoroacetic acid and mixtures incubated on ice for 30 min. Prior to injection on the HPLC column, the sample was centrifuged at 13000*g* for 2 min to remove precipitates.

Steady State Analysis (*Initial Rate Method*). For *C. elegans* Pnc1 and Pnc2 (CePNC1 and CePNC2, respectively), the GDH-coupled assay described above was used to determine the steady state kinetic parameters. Reactions were conducted in a 150 μL total volume containing varying concentrations of nicotinamide (0, 10, 20, 30, 40, 50, 75, 100, 200, 400, and 600 μM) on a 96-well plate. The reactions were initiated by addition of nicotinamidase (final concentrations of 500 nM CePNC1 and 667 nM CePNC2), and the decreasing fluorescence intensity was monitored with a microplate reader for a total of 900 s at 27 s intervals. The initial rates of reactions were derived from the slopes of the amount of product formed versus time where the extent of reaction had not exceeded 15% of the substrate in each case. Determined rates were plotted versus nicotinamide concentrations and fit with the Michaelis−Menten equation using Kaleidagraph (Synergy Software).

Steady State Progress Curve Analysis. For SpNic and Pnc1, kinetic parameters were measured by the GDH-coupled assay described above and calculated by progress curve analysis. Reactions were conducted in a 600 μL total volume containing 100 μM nicotinamide in UV cuvettes. The reactions were initiated by addition of nicotinamidase (final concentrations of 200 nM Pnc1 and 12 nM SpNic). The absorbance at 340 nm was monitored with a UV spectrophotometer over a total of 60 min at 22 s intervals for SpNic and 15 min at 25 s intervals for Pnc1. Progress curve analysis involved approximating instantaneous rates at a time t_x, where product formation at t_{x-1} and t_{x+1} was determined and the $\Delta P/\Delta t$ was calculated to determine the instantaneous rate. t_x represents the mid-time point between t_{x-1} and t_{x+1}, and t_{x-1} and t_{x+1} represent the start and end points of the time interval, respectively. Rates were plotted versus substrate concentration (at each time where instantaneous rate was calculated) and the data was fit to the Michaelis−Menten equation to determine K_m and k_{cat} values. The method is similar to that published for this approach (*38*).

Steady State Kinetics−HPLC Analysis. For BbNic the HPLC assay described above was used to measure the steady state kinetic parameters. Nicotinamide was incubated at concentrations of 0, 20, 40, 60, 80, 120, 160, 200, and 400 μM, with 5.4 μM enzyme. Chromatograms were analyzed at a wavelength of 260 nm. Reactions were quantified by integrating areas of peaks corresponding to nicotinamide and nicotinic acid. Rates were plotted versus nicotinamide concentration, and a curve fit of the points to the Michaelis−Menten equation was performed with Kaleidagraph to determine the kinetic parameters.

For *Pl. falciparum* nicotinamidase, reactions that included 0, 2.5, 3.75, 5, 7.5, 10, 20, 25, and 50 μM nicotinamide with 20% [*carbonyl*-C^{14}]nicotinamide in 100 mM phosphate buffer (pH 7.3) were initiated with the addition of PfNic; reaction mixtures were incubated for 7 min, and reactions were quenched by addition of 8 μL of 10% trifluoroacetic acid. After centrifugation at 13000*g* for 2 min, the reaction mixtures were injected onto an HPLC column as described above to separate nicotinamide and nicotinic acid. Eluents containing nicotinamide and nicotinic acid were collected, and radioactivity was determined by scintillation counting. Rates were determined as counts per minute per second and then converted to a turnover rate (s^{-1}) by adjustment for the specific radioactivity of nicotinamide and enzyme concentration. Rates were plotted versus nicotinamide concentration, and a best fit of the plotted data to the Michaelis−Menten equation was performed with Kaleidagraph.

Inhibition Analysis. To assess inhibition, reactions were performed using the GDH-coupled assay described above. Reactions that included 1 mM α-ketoglutarate, 250 μM NAD(P)H, 1.5 units of GDH per 100 μL of reaction volume, either 200 μM or 2 mM nicotinamide, and varying concentrations of inhibitors in 100 mM phosphate buffer (pH 7.3) were initiated with the addition of nicotinamidases. Rates were plotted and points fit to eq 1 using Kaleidagraph:

$$v_{inh}/v_0 = ([S] + K_m)/[[S] + K_m(1 + [I]/K_i)] \quad (1)$$

where v_{inh} is the inhibited rate for a given concentration of inhibitor, v_0 is the uninhibited rate, [S] is the nicotinamide concentration, K_m is the Michaelis constant for nicotinamide for the nicotinamidase, [I] is the inhibitor concentration, and K_i is the intrinsic binding constant for competitive inhibition. In most cases, the inhibition data were fit to Morrison's quadratic equation and in all cases where inhibitors were found to have an intrinsic K_i of < 5 μM (eq 2):

$$v_{inh}/v_0 = 1 - \left[[E]_T + [I]_T + K_i^{app} - \sqrt{([E]_T + [I]_T + K_i^{app})^2 - 4[E]_T[I]_T}\right]/(2[E]_T) \quad (2)$$

where v_{inh} is the inhibited rate for a given concentration of inhibitor, v_0 is the uninhibited rate, $[E]_T$ is the total enzyme concentration, $[I]_T$ is the total inhibitor concentration, and K_i^{app} is the apparent inhibition constant as described previously (*39*). K_i, the intrinsic binding constant for binding of the inhibitor to the enzyme, can be calculated from K_i^{app} by the relation (eq 3)

$$K_i = K_i^{app}/(1 + [S]/K_m) \quad (3)$$

where [S] is the substrate concentration and K_m is the Michaelis constant for binding of the substrate to the enzyme as described previously (*39*).

Competition Analysis of Inhibitors. Nicotinaldehyde was characterized as an inhibitor versus nicotinamide. Use of the GDH-coupled assay described above was used for the competitive analysis. Inhibition reactions were performed in 150 μL containing 1 mM α-ketoglutarate, 250 μM NADPH, 2.25 units of GDH, and different concentrations of nicotinamide (50, 100, 250, 500, and 1000 μM) in 100 mM phosphate buffer (pH 7.3), with inhibitor concentrations 0, 2, or 5 times the estimated K_i as indicated in Figure 5. Reactions were initiated by addition of nicotinamidase enzymes (typically 20−100 nM). Double-reciprocal plots of $1/v$ versus 1/[nicotinamide] at different fixed concentrations of the inhibitor were plotted, where v is the observed rate. Intersection of the lines on the $1/v$ axis indicated competitive inhibition. All data points were fit to the double-reciprocal equation for competitive inhibition using Kaleidagraph.

Nicotinamidase Activity of Mutants. To determine the catalytic rate of SpNic and its mutants, reactions that included 200 μM nicotinamide were conducted at pH 7.5 and 37 °C using standard assay conditions for HPLC as described elsewhere in

this section; one of the following: 100 nM SpNic wild type (wt), 100 nM R97A, 5 μM K103A, 5 μM C136A, or 5 μM C136S was used in each reaction. Reactions were quenched with 10% TFA. Nicotinic acid was separated from nicotinamide by HPLC and quantified. The catalytic rates of SpNic and the R97A mutant were also determined by a plate assay as described elsewhere in this section at 37 °C. In HPLC assays, the observed catalytic rates of K103A, C136A, and C136S were determined from product formation after a 1 h reaction. Similar reaction rate analyses were performed in each case with 1 mM nicotinamide.

^{18}O Isotope Exchange Catalyzed by S. pneumoniae Nicotinamidase. To obtain a fully equilibrated nicotinic acid with ^{18}O content in water, 25 μL reaction mixtures in 40 mM phosphate buffer (pH 7.0) containing $H_2{}^{18}O$ (to a final ^{18}O content of 87%), 1 mM nicotinic acid, and 6 μM SpNic were incubated for 0 (prequenched), 2, 10, 30, and 60 min at 37 °C and reactions were quenched with 4 μL of 10% trifluoroacetic acid. A reaction with no enzyme was run as a control and quenched identically at 60 min. Twenty microliters of each reaction mixture was injected onto a C-18 reverse phase column (EC250/4.6 NUCLEODUR 100-5 C18, Macherey-Nagel) to separate nicotinic acid using 20 mM ammonia acetate (pH 7.0) as the eluant. Eluant containing nicotinic acid was dried by lyophilization and redissolved in 10 μL of water; 1 μL of sample was spotted on a gold MALDI plate, and 1 μL of matrix composed of 10 mg/mL α-cyano-4-hydroxycinnamic acid (CHCA) and 0.1% TFA (50:50, v/v) was added and dried. The mass spectrum was recorded with an Applied Biosystems DE-STR MALDI-TOF spectrometer (Proteomics Resource Center, Rockfeller University, New York, NY). For each sample, the mass spectrum was recorded through 200 shots and the measurement repeated three times and averaged. [U-^{16}O]Nicotinic acid was detected at m/z 124.07(5), which is the mass of the twice-protonated species. [^{16}O,^{18}O]Nicotinic acid was detected at m/z 126.07(5), and [U-^{18}O]-nicotinic acid was detected at m/z 128.07(5). Complete equilibrative exchange of ^{18}O into nicotinic acid was observed after 1 h, and significant exchange was measured at 2 min. No exchange was observed in the sample that received no enzyme. Formation of [^{18}O]nicotinic acids (singly and doubly labeled) was confirmed by HRMS (CUNY Hunter Mass Spectrometry Facility). Predicted mass for singly labeled [^{18}O]nicotinic acid ($C_6H_5NO[^{18}O]$): m/z calcd 125.0363, found 125.0365. Predicted mass for doubly labeled [^{18}O]nicotinic acid ($C_6H_5N[^{18}O]_2$): m/z calcd 127.0405, found 127.0407.

To determine the rate of exchange with $H_2{}^{18}O$, we used the initial rate method. Reaction mixtures with a volume of 25 μL in 40 mM phosphate buffer (pH 7.0) containing $H_2{}^{18}O$ (to a final ^{18}O content of 87%), 1 mM nicotinic acid, and 100 nM SpNic were reacted for 0, 20, 40, 60, and 120 min and quenched and processed as described above. The ^{18}O isotope-incorporated nicotinic acids at m/z 126 and 128 were detected with a MALDI-TOF spectrometer, and their combined intensity expressed as a percentage was plotted and fit to a linear curve versus time. The rate data was converted to an observed exchange rate constant for the reaction conditions by taking into account enzyme concentration and nicotinic acid concentrations in the sample. The observed exchange rate constant was corrected to the intrinsic rate constant of exchange by eq 4:

$$k_{obs}(\text{corrected}) = k_{obs}/0.87 \quad (4)$$

where k_{obs} is the experimentally determined rate constant of exchange, 0.870 is the mole fraction of ^{18}O isotope in water, and k_{obs}(corrected) is the observed rate constant corrected for the isotope mole fraction.

The exchange rates of mutant SpNic enzymes were measured using 1 mM NA in reaction mixtures with a volume of 25 μL in 40 mM phosphate buffer (pH 7.0) containing $H_2{}^{18}O$ (to a final ^{18}O content of 87%); one of the following: 100 or 500 nM SpNic wt, 500 nM R97A, 5 μM K103A, or 5 μM C136A was used in each reaction. The observed exchange rates of SpNic wt and R97A were determined by the initial rate method for a 30 min reaction at 37 °C; the observed exchange rates of K103A and C136A were determined from a 2 h reaction at 37 °C. The ^{18}O isotope-incorporated nicotinic acids at m/z 126 and 128 were detected with a MALDI-TOF spectrometer, and their combined intensity percentage was used to calculate the observed exchange rate with correction for the isotope fraction of ^{18}O in water as described above.

Synthesis of Substrate Analogues. Nicotinamide, 2-chloronicotinamide, 6-chloronicotinamide, 6-methylnicotinamide, 6-aminonicotinamide, isonicotinamide, and ethyl nicotinate were purchased from Aldrich. Thionicotinamide was purchased from Acros. We also thank P. Tyler of IRL New Zealand for several samples of nicotinamides, including 5-methylnicotinamide, 6-chloronicotinamide, 6-methylnicotinamide, and 6-aminonicotinamide. 5-Methylnicotinamide was alternatively synthesized as reported previously (*40*).

5-Methoxynicotinamide was synthesized from the corresponding aldehyde (*41*). 5-Methoxy-3-pyridinecarboxaldehyde (400 mg, 2.92 mmol) was dissolved in 4 mL of methanol and to this solution was added hydroxylamine hydrochloride (264 mg, 3.80 mmol). The reaction mixture was allowed to stir at 25 °C for 4 h. Solvent was removed under reduced pressure; the residue was redissolved in 3 mL of dry pyridine, and to this solution was added methanesulfonyl chloride (435 mg, 3.80 mmol). The mixture was stirred at 25 °C for 2 h, and then water and ethyl acetate were added. The combined organic layer was dried over Na_2SO_4. Column chromatography (4:1 hexanes/ethyl acetate) afforded 320 mg (2.39 mmol, 82% yield) of 3-cyano-5-methoxypyridine as a white solid: ^{1}H NMR (400 MHz, $CDCl_3$) δ 8.49 (d, J = 2.8 Hz, 1H), 8.46 (d, J = 1.5 Hz, 1H), 7.37 (dd, J = 1.6, 2.8 Hz, 1H), 3.89 (s, 3H). Hydrogen peroxide (4 mL) was added dropwise to a solution of 3-cyano-5-methoxypyridine (320 mg, 2.39 mmol) and K_2CO_3 (790 mg, 5.72 mmol) in 3 mL of DMSO, and the mixture was stirred for 1 h before it was diluted with water and lyophilized to dryness. The crude product was purified by column chromatography (10:1 ethyl acetate/ethanol) followed by recrystallization in ethyl acetate to afford 200 mg (1.32 mmol, 55% yield) of 5-methoxynicotinamide as a white solid: ^{1}H NMR (400 MHz, DMSO) δ 8.62 (d, J = 1.7 Hz, 1H), 8.40 (d, J = 2.9 Hz, 1H), 8.13 (s, br, 1H), 7.74 (dd, J = 1.8, 2.8 Hz, 1H), 7.59 (s, br, 1H), 3.86 (s, 3H); ^{13}C NMR (100 MHz, DMSO) δ 55.7, 118.8, 130.3, 140.1, 140.7, 155.0, 166.2; HRMS (ESI) calcd for $C_7H_8N_2O_2$ 152.0586, found 152.0587.

4-Methoxynicotinamide was synthesized from the corresponding aldehyde (*41*). 4-Methoxy-3-pyridinecarboxaldehyde (180 mg, 1.31 mmol) was dissolved in 2 mL of methanol and to this solution was added hydroxylamine hydrochloride (118 mg, 1.70 mmol). The reaction mixture was allowed to stir at room temperature for 4 h. Solvent was removed under reduced pressure; the residue was redissolved in 2 mL of dry pyridine, and to this solution was added methanesulfonyl chloride (195 mg, 1.70 mmol). The mixture was stirred at room temperature for 2 h, and then water and ethyl acetate were added. The combined organic layer was dried over Na_2SO_4. Column chromatography (1:2 hexanes/ethyl acetate) afforded 135 mg (1 mmol, 78% yield) of 3-cyano-4-methoxypyridine as a white solid: ^{1}H NMR (400 MHz, $CDCl_3$)

δ 8.67 (s, 1H), 8.62 (d, J = 6.0 Hz, 1H), 6.90 (d, J = 6.0 Hz, 1H), 3.99 (s, 3H). Hydrogen peroxide (1.67 mL) was added dropwise to a solution of 3-cyano-4-methoxypyridine (135 mg, 1 mmol) and K_2CO_3 (333 mg, 2.4 mmol) in 3 mL of DMSO, and the mixture was stirred for 1 h before it was diluted with water and lyophilized to dryness. The crude product was purified by column chromatography (10:1 ethyl acetate/ethanol) followed by recrystallization in ethyl acetate to afford 100 mg (0.66 mmol, 66% yield) of 4-methoxynicotinamide as a white solid: ^{1}H NMR (400 MHz, DMSO) δ 8.70 (s, 1H), 8.51 (d, J = 5.8 Hz, 1H), 7.64 (s, br, 1H), 7.61 (s, br, 1H), 7.15 (d, J = 5.9 Hz, 1H), 3.93 (s, 3H); ^{13}C NMR (125 MHz, DMSO) δ 57.0, 108.7, 117.7, 151.5, 154.2, 165.2, 168.9; HRMS (ESI) calcd for $C_7H_8N_2O_2$ 152.0586, found 152.0587.

2-Aminoisonicotinamide was synthesized as described previously (*42*) with several modifications. Briefly, acetylation of 2-amino-4-picoline followed by oxidation using $KMnO_4$ gave 2-*N*-acetylamidoisonicotinic acid. This compound was subjected to amidation in the presence of DCC and ammonia in methanol to yield 2-*N*-acetylamidoisonicotinamide. Further reaction of 2-*N*-acetylamidoisonicotinamide with ammonia in methanol provided the desired 2-aminoisonicotinamide in modest yield; ^{1}H NMR matches reported data.

Phenyl nicotinate was synthesized from nicotinoyl chloride hydrochloride. To a 100 mL round-bottom flask were added nicotinoyl chloride hydrochloride (770 mg, 4.33 mmol), 5 mL of triethylamine, and 20 mL of THF. To this mixture was added 4 mL of pyridine dropwise. After the mixture had been stirred for 30 min at 25 °C, phenol (610 mg, 6.49 mmol) was added. The reaction mixture was kept at 25 °C overnight; the precipitate was filtered off, and the solution was evaporated under reduced pressure. The residue was redissolved in water and extracted with CH_2Cl_2. The combined organic layer was washed with brine and dried over anhydrous Na_2SO_4. Solvent was then concentrated in vacuo, and crude product was recrystallized from ethyl acetate: ^{1}H NMR (500 MHz, $CDCl_3$) δ 9.41 (s, 1H), 8.86 (dd, J = 1.7, 4.9 Hz, 1H), 8.46 (dt, J = 2.0, 8.0 Hz, 1H), 7.47 (stack, 3H), 7.32 (t, J = 7.3 Hz, 1H), 7.23 (m, 2H).

1-Methylnicotinamide was synthesized using a method similar to that reported by Martin and Hull (*43*). Briefly, 3 equiv of iodomethane was added to a solution of nicotinamide in 2 mL of methanol. The reaction mixture was allowed to stir at room temperature and monitored by TLC. When the reaction was complete (after approximately 30 h), the solid was filtered off and dried under reduced pressure. The resulting product was purified by recrystallization from methanol: ^{1}H NMR (500 MHz, DMSO) δ 9.4 (s, 1H), 9.11 (d, J = 6.1 Hz, 1H), 8.90 (d, J = 8.2 Hz, 1H), 8.51 (s, br, 1H), 8.25 (dd, J = 6.1, 8.1 Hz, 1H), 8.14 (s, br, 1H), 4.42 (s, 3H). 1-Methylisonicotinamide was prepared similarly.

Synthesis of Inhibitors. 3-Pyridinecarboxaldehyde, 5-bromo-3-pyridinecarboxaldehyde, 2-chloro-3-pyridinecarboxaldehyde, 3,5-lutidine, 3,5-dibromopyridine, 4-methoxypyridine, 3-cyanopyridine, 3-acetylpyridine, 3-hydroxypyridine, and nicotinic acid were purchased from Aldrich.

5-Methoxy-3-pyridinecarboxaldehyde was synthesized in two steps from 3,5-dibromopyridine (*44*). Sodium methoxide in methanol (4 mL, 9.56 mmol) was stirred under reduced pressure at 65 °C for 10 min. The remaining solid was dissolved in 5 mL of DMF. Solid 3,5-dibromopyridine (1.5 g, 6.33 mmol) was added, and the mixture was stirred at 63−68 °C for 1 h. Then it was poured into water and extracted with ethyl acetate. The combined organic layer was washed with brine and dried over anhydrous Na_2SO_4. After the solvent was evaporated under reduced pressure, column chromatography afforded 1 g (5.32 mmol, 85% yield) of 3-bromo-5-methoxypyridine as a white solid: ^{1}H NMR (400 MHz, $CDCl_3$) δ 8.31 (s, 1H), 8.26 (s, 1H), 7.35 (s, 1H), 3.88 (s, 3H). To a stirred solution of 3-bromo-5-methoxypyridine (1 g, 5.3 mmol) in 20 mL of anhydrous THF at −90 °C was added *n*BuLi (2.9 mL, 5.8 mmol) over 5 min. The solution was allowed to stir for an additional 20 min at −90 °C, and then DMF (0.53 mL, 6.9 mmol) was added. The reaction mixture was stirred for 30 min, and the cold mixture was poured directly into brine and extracted with ethyl acetate. The combined organic layer was dried over anhydrous Na_2SO_4. After solvent was evaporated under reduced pressure, column chromatography afforded 0.5 g (3.65 mmol, 68% yield) of 5-methoxy-3-pyridinecarboxaldehyde as a pale yellow solid: ^{1}H NMR (400 MHz, $CDCl_3$) δ 10.08 (s, 1H), 8.63 (d, J = 1.5 Hz, 1H), 8.53 (d, J = 3 Hz, 1H), 7.58 (dd, J = 1.5, 3 Hz, 1H), 3.89 (s, 3H).

5-Methyl-3-pyridinecarboxaldehyde was synthesized in three steps from 3,5-lutidine. 3,5-Lutidine was converted to 5-methylnicotinic acid as described previously (*45*). 5-Methylnicotinic acid (100 mg, 0.73 mmol), triphenylphosphine (382 mg, 1.46 mmol), and methanol (47 mg, 1.46 mmol) were dissolved in 1 mL of anhydrous THF, and to this solution was added DIAD (295 mg, 1.46 mmol) at 0 °C dropwise. The reaction mixture was allowed to warm to room temperature and stir overnight. Saturated brine was added to quench the reaction, and the aqueous layer was extracted with ethyl acetate. The combined organic layer was dried over anhydrous Na_2SO_4 and concentrated under reduced pressure. The crude product was purified by column chromatography to afford 70 mg (0.46 mmol, 64% yield) of 5-methylnicotinic acid methyl ester as a white solid: ^{1}H NMR (500 MHz, $CDCl_3$) δ 9.01 (s, 1H), 8.59 (s, 1H), 8.09 (s, 1H), 3.93 (s, 3H), 2.38 (s, 3H). To a solution of 5-methylnicotinic acid methyl ester (70 mg, 0.46 mmol) in 2 mL of toluene was added DIBAL-H (3.2 mL, 3.2 mmol) dropwise at −78 °C. The reaction mixture was kept at −78 °C for 1 h before the reaction was quenched by methanol at −20 °C. To the reaction mixture were then added 0.1 M HCl and ether; the aqueous phase was extracted with ether, and the combined organic phase was washed with saturated $NaHCO_3$, water, and brine and then dried over anhydrous Na_2SO_4. Solvent was evaporated under reduced pressure, and the crude product was purified by column chromatography to afford 50 mg (0.41 mmol, 89% yield) of 5-methyl-3-pyridinecarboxaldehyde as a colorless oil: ^{1}H NMR (500 MHz, $CDCl_3$) δ 10.08 (s, 1H), 8.87 (s, 1H), 8.67 (s, 1H), 7.95 (s, 1H), 2.43 (s, 3H).

6-Fluoro-3-pyridinecarboxaldehyde was synthesized from the corresponding carboxylic acid. In general, the acid was reduced with 1.1 equiv of lithium aluminum hydride in refluxing anhydrous THF overnight. After the reaction had been quenched with ethyl acetate and water, the precipitate was filtered off, the solvent was removed under reduced pressure, and the alcohol was used for the next step without further purification. The alcohol was added to 2 equiv of sodium nitrite followed by 1 equiv of acetic anhydride and the mixture stirred at 0 °C (*46*). The reaction was monitored by TLC, and upon completion, the product was extracted with diethyl ether. The aldehyde was further purified by column chromatography: ^{1}H NMR (500 MHz, $CDCl_3$) δ 10.08 (s, 1H), 8.75 (d, J = 1.5 Hz, 1H), 8.32 (dt, J = 2.1, 8.2 Hz, 1H), 7.11 (dd, J = 2.5, 8.4 Hz, 1H); ^{13}C NMR (125 MHz, DMSO) δ 110.6, 110.9, 114.1, 139.3, 140.9, 141.0, 152.0, 152.1, 188.6; HRMS (ESI) calcd for C_6H_4FNO 125.0277, found 125.0281.

4-Methoxy-3-pyridinecarboxaldehyde was synthesized in one step from 4-methoxypyridine (*44*). To a solution of *t*BuLi

Scheme 3: The Nicotinamidase Assay Developed Here Couples the Release of Ammonia to the Consumption of NAD(P)H via Glutamate Dehydrogenase[a]

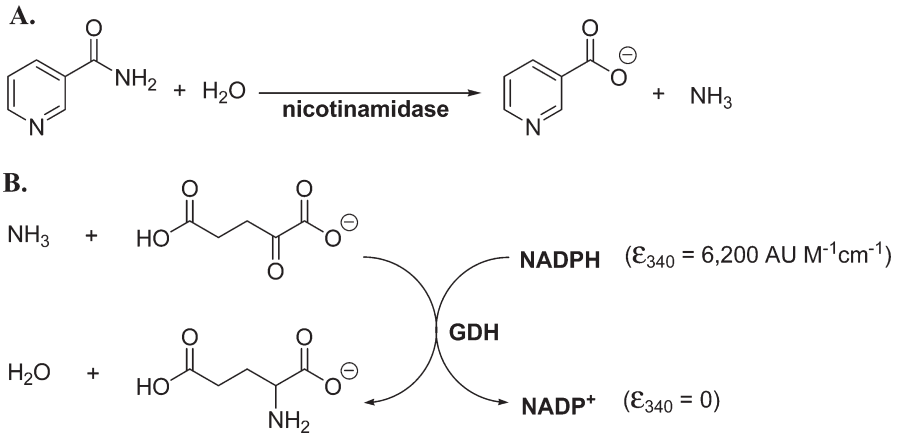

[a]The synthesis of glutamate by GDH occurs in the presence of ammonia and α-ketoglutarate and is dependent upon the stoichiometric oxidation of NAD(P)H. The conversion of NAD(P)H to NAD(P)$^+$ can be followed by monitoring the decrease in absorbance at 340 nm or the decrease in fluorescence (excitation at 360 nm and emission at 490 nm).

(1.7 M in pentane, 16.6 mL, 28 mmol) in 30 mL of anhydrous THF at −78 °C was added 2.2 g of 2-bromomesitylene (1.66 mL, 11 mmol). After the mixture had been stirred at −78 °C for 1 h, a pale yellow heterogeneous mixture was formed. To this mixture was then added 1.09 g of 4-methoxypyridine (1 mL, 10 mmol), and stirring was continued at −78 °C for 1 h, at −23 °C for 1 h, and at room temperature for 1 h. The mixture was again cooled to −78 °C, and 0.954 g of DMF (1 mL, 13.1 mmol) was added dropwise. After the mixture had been stirred at −78 °C for an additional 1 h, the reaction was quenched with a saturated $NaHCO_3$ solution. The aqueous layer was extracted with ethyl acetate (3 × 10 mL), and organic layers were combined and dried over anhydrous Na_2SO_4. After the solvent had been evaporated under reduced pressure, column chromatography afforded 0.88 g (6.4 mmol, 64% yield) of 4-methoxy-3-pyridinecarboxaldehyde as a pale yellow solid: ^{1}H NMR (400 MHz, $CDCl_3$) δ 10.42 (s, 1H), 8.86 (s, 1H), 8.61 (d, J = 6 Hz, 1H), 6.91 (d, J = 6 Hz, 1H), 3.98 (s, 3H).

RESULTS

Cloning and Protein Expression. The genes encoding the nicotinamidase enzymes from *B. burgdorferi* (BbNic), *S. pneumoniae* (SpNic), and *Pl. falciparum* (PfNic) were cloned into appropriate expression vectors and expressed and purified as described in Materials and Methods and the Supporting Information. Expression plasmids for the two *C. elegans* nicotinamidases, CePNC1 and CePNC2 (*12*), and *Sa. cerevisiae* Pnc1 (*24*) were previously described. When assayed by HPLC under standard reaction conditions [200 μM nicotinamide and 100 mM phosphate (pH 7.3)], all enzymes were found to catalyze the conversion of nicotinamide into nicotinic acid (Supporting Information).

Nicotinamidase Assay Development. To monitor the activity of purified enzymes in real time, we developed a robust and straightforward assay that could continuously monitor one of the two products of the nicotinamidase reaction, ammonia. Bovine glutamate dehydrogenase (GDH), which is commercially available, was found to be an ideal enzyme for this purpose. GDH catalyzes the reaction of α-ketoglutarate, ammonia, and NADPH (or NADH) to form glutamate and the oxidized dinucleotide (Scheme 3). The ammonia produced by conversion of nicotinamide to nicotinic acid is reacted by the coupling enzyme, which in turn consumes NADPH stoichiometrically. Conversion of NADPH to NADP$^+$ can be measured by absorbance of NADPH at a wavelength of 340 nm where NADP$^+$ has no absorbance ($\Delta\varepsilon_{340}$ = 6200 AU M^{-1} cm^{-1}). Alternatively, the method was readily adapted to a plate reader that can detect fluorescence emission of NADPH (excitation at 360 nm and emission at 490 nm). NADPH is measured by the amount of emitted light and rates determined by changes in light emission versus time. Both methods were used to monitor nicotinamidase activity in this study.

The quantity of NADPH consumed correlates well with the quantities of nicotinamide or ammonia added to a sample as shown in panels A and B of Figure 2. In addition, the rate of nicotinamidase activity scales linearly with the amount of enzyme added, demonstrating that the coupling enzyme can be provided so that GDH is not limiting for the determination of catalytic velocity (Figure 2C). This assay is effective for monitoring a wide range of nicotinamide concentrations and can accurately detect rates generated by low micromolar concentrations of nicotinamide, particularly because of the low GDH K_m for NADPH (28 μM) and an excellent rate of turnover (>9 s^{-1}, calculated from kinetic parameters) (*47*). Favorably, the equilibrium position very strongly favors the oxidized dinucleotide product at pH 7.0 (*48*). Interference of GDH from nicotinamide and nicotinic acid was neglible, and the components of the GDH assay did not interfere with nicotinamidase enzymatic activity as determined by HPLC (data not shown). The components of this assay, nicotinamidase and GDH, were recently combined in a coupled assay for the detection and measurement of the activity of nicotinamide-forming enzymes, such as sirtuins, that degrade NAD$^+$ to nicotinamide (*49*).

Kinetics Parameters for Nicotinamidase Enzymes. Kinetic properties of nicotinamidase enzymes cloned or isolated from a variety of organisms have been determined previously, including *Arabidopsis thaliana* (*9*), *M. tuberculosis* (*3*), *Mycobaceterium smegmatis* (*2*), *Lactobaccillus arabinosis* (*32*, *50*), *Torula cremoris* (*7*), *Flavobacterium peregrinum* (*51*), and *Sa. cerevisiae* (*5*, *6*, *52*, *53*). Of the enzymes considered in this study, the nicotinamidase activity of the *Pl. falciparum* enzyme was previously detected in crude dialyzed lysates derived from *Pl. falciparum*-infected erythrocytes (*8*). With a reliable assay available, we sought to

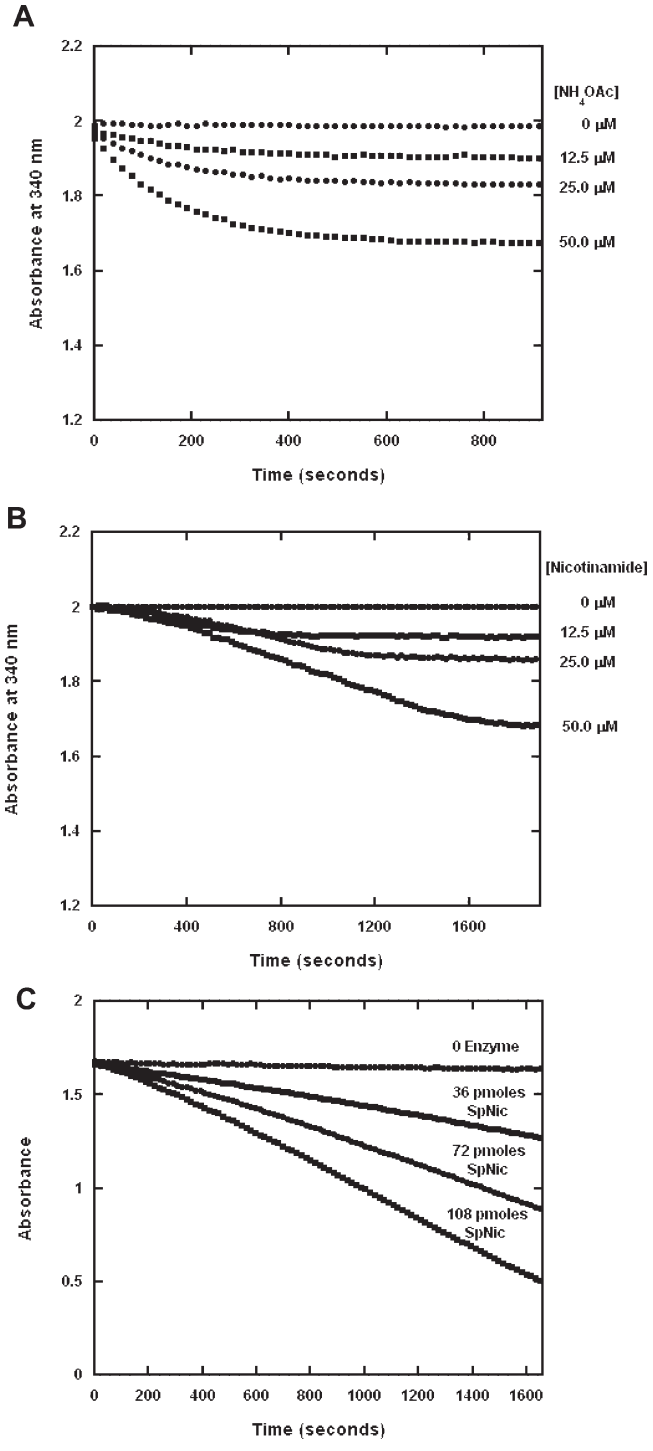

FIGURE 2: (A) GDH assay performed with varying concentrations of ammonium acetate. (B) GDH-coupled assay performed with varying concentrations of nicotinamide. Reactions that included 1 mM α-ketoglutarate, 250 μM NADPH, and 1.5 units of GDH per 100 μL of reaction volume in 100 mM phosphate buffer (pH 7.3) were initiated with the addition of PfNic to a final concentration of 320 nM. The reactions were measured by monitoring the absorbance at 340 nm over time. (C) SpNic activity scales with varying concentrations of enzyme. Reactions that included 1 mM α-ketoglutarate, 250 μM NADPH, and 1.5 units GDH per 100 μL of reaction volume in 100 mM phosphate buffer (pH 7.3) were initiated with the addition of SpNic to the amounts indicated in the figure. The reactions were measured by monitoring the absorbance at 340 nm over time. The slopes for 0, 36, 72, and 108 pmol of SpNic are -2.23×10^{-5}, -2.39×10^{-4}, -4.79×10^{-4}, and -7.30×10^{-4}, respectively.

determine the kinetic parameters for the *Sa. cerevisiae* Pnc1 as the prototype enzyme. In addition, the kinetic parameters for the *S. pneumoniae*, *B. burgdorferi*, *Pl. falciparum*, and both *C. elegans* nicotinamidases were determined for the first time. Enzymes were expressed in *E. coli* and isolated by Ni^{2+} column chromatography. Although different enzymes from different sources have been reported to have different central metal requirements (*3*, *9*, *34*), enzymes were active as purified without being reconstituted from the apo form. However, we did examine the addition of metal ions to the purified enzymes, and in almost every case, no change in activity was observed (see Table S1 of the Supporting Information). We did not attempt to investigate the identity of the coordinated central metal atom for the respective enzymes, although SpNic was recently reported to prefer Zn^{2+} (*35*) and the preferred metal for the yeast enzyme is reportedly Zn^{2+} as well (*6*). Interestingly, addition of Zn^{2+} to reaction mixtures did not appreciably change the catalytic activity of any nicotinamidase, although the SpNic and CePNC2 enzymes were moderately stimulated by Mn^{2+} added to reaction mixtures (see the Supporting Information).

Employing standard assay conditions [100 mM potassium phosphate (pH 7.3), we determined steady state kinetic parameters for each enzyme. In most cases, the nicotinamide concentration was varied and initial rates versus the concentration of nicotinamide were plotted and curve fit to determine K_m and k_{cat} values (Figure 3 and Table 1). k_{cat} was also measured by the HPLC assay using a concentration of nicotinamide of at least $10K_m$ for confirmation.

For the Pnc1 and SpNic enzymes, progress curve analysis was used (*38*), which allowed sensitivity to low concentrations of substrate. This was important because of a low K_m for nicotinamide for these enzymes. A potential caveat with these analyses is product inhibition, which can increase the apparent K_m, but we showed that nicotinamidase rates for all enzymes do not vary when concentrations of nicotinic acid up to 500 μM are present (data not shown) and nicotinic acid is thermodynamically stable relative to substrate, so the reaction invariably goes to completion. Pnc1 and SpNic were determined to have K_m values of 10 and 2.7 μM, respectively, for nicotinamide and corresponding k_{cat} values of 3.8 and 2.1 s^{-1}, respectively.

For other nicotinamidases, we used the GDH method (CePNC1 or CePNC2) or an HPLC method (PfNic and BbNic) to determine initial reaction rates as a function of nicotinamide concentration. All data are summarized in Table 1. All K_m values were found to be below 120 μM, with k_{cat} values in the range of 0.3−4 s^{-1}. Only BbNic deviated from the pattern. An examination of the BbNic sequence against the others (Figure 1) shows that the genetically encoded enzyme is approximately 20 residues (*51*) shorter at the N-terminus. This region contains a highly conserved DXQXD sequence that is highly conserved in nicotinamidases (Figure 1). Thus, we introduced additional sequence at the N-terminus to create an active enzyme [as originally reported (*19*)]. It remains possible that BbNic is imperfectly reconstituted in sequence or in other requirements, accounting for its poor catalytic properties [introduction of different metal ions had no effect on activity (see the Supporting Information)].

Substrate Specificity. We probed the specificity of nicotinamidases in hydrolyzing a variety of nicotinamide analogues. Using both HPLC analysis and the GDH-coupled assay, we determined the relative rates for a number of compounds showing structural similarity to nicotinamide (Table 2). In the cases of SpNic, Pnc1, and PfNic, substitutions at the 5-position were well tolerated, and interestingly, 5-methyl, **1**, and 5-*O*-methyl substitution, **2**,

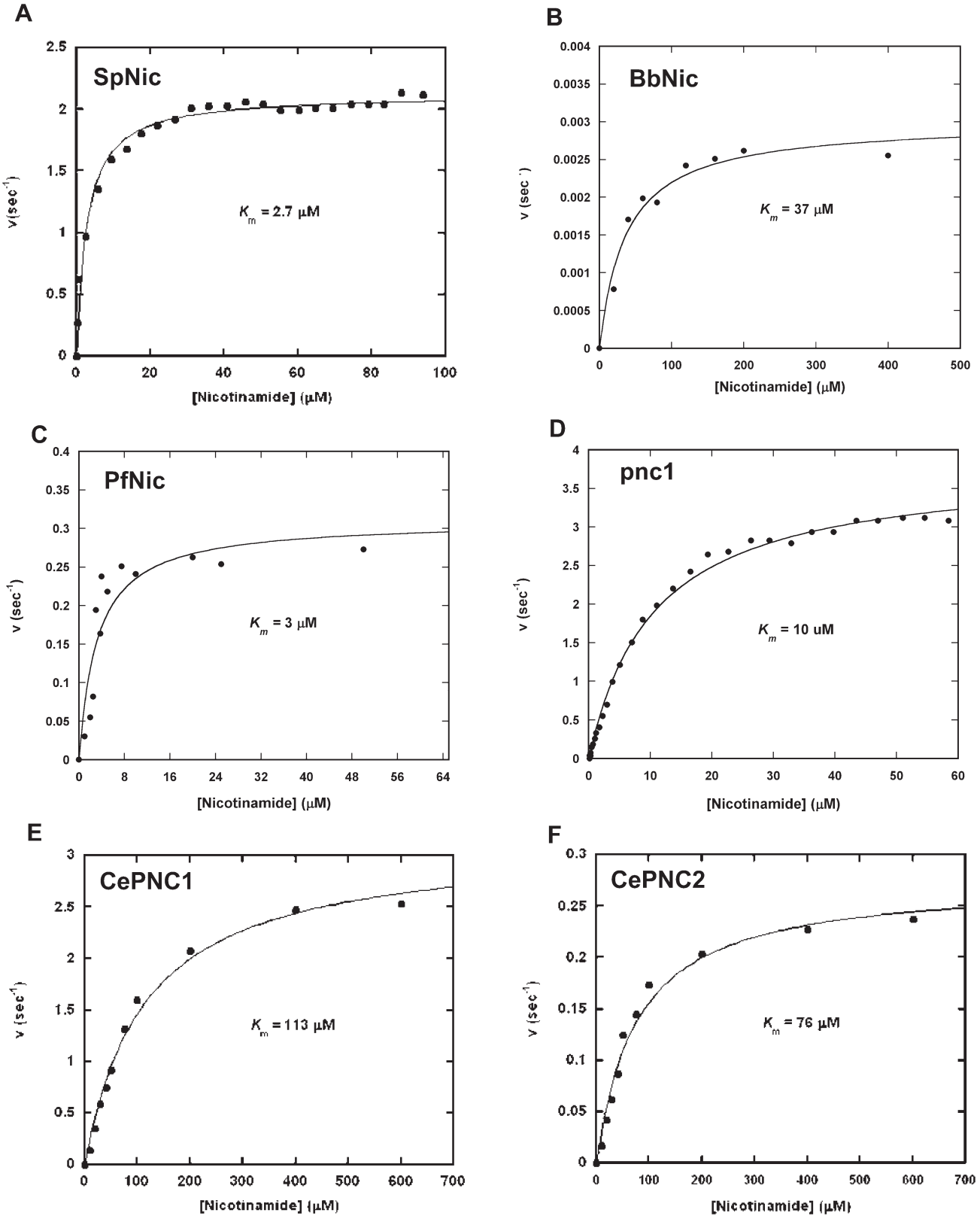

FIGURE 3: Steady state saturation curves of nicotinamidases from *Sa. cerevisiae* (A), *B. burgdorferi* (B), *Pl. falciparum* (C), and *S. pneumoniae* (D) and *C. elegans* Pnc1 (E) and Pnc2 (F). Panels A and D were derived from progress curve analysis (see Materials and Methods) of the nicotinamidase reaction run in the presence of 100 μM nicotinamide; panels B and C are from HPLC analysis of reactions run at varying nicotinamide concentrations, and panels E and F are from the GDH-coupled fluorescence assay with various concentrations of nicotinamide. In all cases, the data were fit to the Michaelis−Menten equation using KaleidaGraph.

caused an up to 6.5-fold rate enhancement [in k_{cat} (see Table 2)] over that of nicotinamide. Moving the *O*-methyl group to the 4-position, **7**, caused slowing of all enzymes to 5−12% of the rate observed for nicotinamide (Table 2). Nicotinamidases (BbNic, PfNic, Pnc1, and SpNic) could not hydrolyze isonicotinamides **8**, **9**, 1-methylisonicotinamide, **15**, or 1-methylnicotinamide derivatives [**14** (Table 2)]. These results are consistent with a requirement of coordination of the pyridine to the active site

metal center, as observed in recent X-ray structures (*34*, *35*), and a requirement of a 3-acyl-substitution pattern of the hydrolyzable acyl group relative to the pyridine N1 atom. 2-Chloronicotinamide **3** could not be hydrolyzed, although 6-chloronicotinamide **4** did react as a substrate, albeit slowly, with Pnc1 and SpNic. The steric proximity of the groups at positions 2 and 6 to the coordinating metal as well as weak basicity likely accounts for these substrate behaviors. Consistently, 6-methyl-, 6-amino-, and 6-*O*-methylnicotinamides, **5**–**7**, respectively, were weaker substrates than nicotinamide for all enzymes, probably because of nonoptimal substrate binding to the metal center. However, these substrates reacted faster than the 6-chloro derivative probably because they are better metal ligands than the halogenated analogue. Nicotinate esters, such as methylnicotinate, **11**, and ethylnicotinate, **12**, could be hydrolyzed efficiently, although not as well as nicotinamide. A notable exception was methylnicotinate. The rate of turnover for methylnicotinate on PfNic was determined to be 65 times faster than that for nicotinamide, with

Table 1: Kinetic Parameters of Nicotinamidases

enzyme	K_m (μM)[a]	k_{cat} (s^{-1})[a]
BbNic	36.7 ± 7.5	0.0030 ± 0.0002[b]
PfNic	3.1 ± 1.2	0.30 ± 0.032[b]
Pnc1	10.6 ± 0.5	3.8 ± 0.1[b]
SpNic	2.7 ± 0.3	2.1 ± 0.1[b]
CePNC1	113 ± 11	3.1 ± 0.12
CePNC2	76 ± 10	0.28 ± 0.013

[a] K_m and k_{cat} values were determined by fitting the data to the Michaelis–Menten equation with Kaleidagraph (Synergy Software). Error values represent the error in the fit to the data as calculated by the curve fitting algorithm. [b] Calculated k_{cat} values were confirmed by the HPLC assay for several enzyme concentrations.

Table 2: Relative Rates of Nicotinamidase Enzymes for Various Nicotinamide Analogues

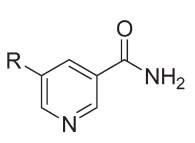

NAM: R = H
1: R = CH_3
2: R = OMe

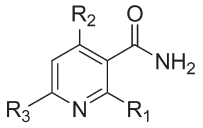

3: R_1 = Cl, R_2, R_3 = H
4: R_1, R_2 = H, R_3 = Cl
5: R_1, R_2 = H, R_3 = CH_3
6: R_1, R_2 = H, R_3 = NH_2
7: R_1, R_3 = H, R_2 = OMe

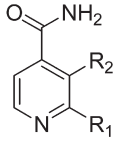

8: R_1, R_2 = H
9: R_1 = NH_2, R_2 = H

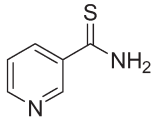

10

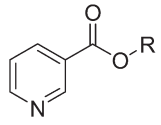

11: R = CH_3
12: R = CH_2CH_3
13: R = Ph

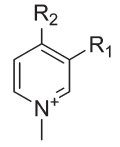

14: R_1 = $CONH_2$, R_2 = H
15: R_1 = H, R_2 = $CONH_2$

substrate	BbNic	PfNic	Pnc1	SpNic
nicotinamide	1.00	1.00	1.00	1.00
1[a]	0.51	3.30	0.80	1.63
2[b]	2.21	6.46	2.06	1.37
3[b]	0	0	0	0
4[b]	0	0	0.17	0.018
5[a]	0.45	0.40	0	0.11
6[a]	ND[c]	0.45	0.20	0.36
7[b]	0.20	0.12	0.050	0.065
8[b]	ND[c]	0	0	0
9[b]	ND[c]	0	0	0
10	0	0	0.44	0
11[b]	ND[c]	65.0	0.15	0.035
12[b]	ND[c]	0.023	0.044	0.0086
13[b]	ND[c]	0.13	0.031	0.031
14[b]	ND[c]	0	0	0
15[b]	ND[c]	0	0	0

[a] Reactions were conducted in a 150 μL total volume containing 1 mM α-ketoglutarate, 250 μM NADPH, 3 units of GDH, and 500 μM nicotinamide analogue in 100 mM phosphate buffer (pH 7.3). Reactions were initiated by addition of nicotinamidase enzymes; the decrease in fluorescence intensity was monitored with a microplate reader. [b] Reactions were conducted in a 25 μL total volume containing 500 μM nicotinamide analogue in 100 mM phosphate buffer (pH 7.3). Reactions were initiated by addition of nicotinamidase enzymes, mixtures incubated 37 °C, and reactions quenched by addition of 10% trifluoroacetic acid. Reactions were analyzed by HPLC. Rates were determined by integrating the area of peaks corresponding to the nicotinic acid analogue. [c] Not determined.

a steady state rate constant of 18 s^{-1}. Interestingly, even phenylnicotinate **13** could be hydrolyzed by SpNic, Pnc1, and PfNic, implying some flexibility of the active site in accommodating this bulkier but activated ester (see the Supporting Information for the NMR study with this substrate and PfNic). Sensitivity to substitutions showed similar trends for the four enzymes for which substrate specificity was broadly evaluated, likely because of structural and mechanistic similarities of these enzymes.

Chemical Exchange of Nicotinic Acid Oxygens with $H_2{}^{18}O$. To evaluate the reversibility of product formation on the SpNic enzyme, we co-incubated nicotinic acid with enzyme in buffered $H_2{}^{18}O$ to test for ^{18}O exchange into the carboxy oxygens of nicotinic acid. The cycling of nicotinic acid to a proposed thioester intermediate (*33*, *34*) and back to nicotinic acid would be predicted to cause a loss of ^{16}O in the carboxy oxygens and replacement with ^{18}O provided water can equilibrate into the active site. We used mass spectrometry to monitor this exchange. As shown in Figure 4B, nearly immediate loss of unlabeled nicotinic acid was observed when 1 mM nicotinic acid was treated with 6 μM SpNic enzyme. This is evident by loss of the *m*/*z* 124 intensity in the MALDI MS spectrum and is accompanied by an increase in intensities for the ions at *m*/*z* 126 and 128. The exchange can be seen to yield equilibration of the substrate oxygens with the initial 87% ^{18}O content in solvent over the course of 1 h, and the relevant equilibria are shown in the scheme accompanying Figure 4. The exchange of the isotope can be observed in as little as 2 min (Figure 4B), and the calculated rate for the process is 0.34 s^{-1} (based on initial rates), indicating it is quite fast at pH 7 (Figure 4C and Table 3). To further confirm that nicotinic acid can be exchanged with $H_2{}^{18}O$ to the extent predicted by the isotopic enrichment, we collected nicotinic acid after incubation with nicotinamidase and $H_2{}^{18}O$ and analyzed it by HRMS, which corroborated these results (see Materials and Methods). The results show that nicotinic acid undergoes facile ^{18}O exchange into the carboxylates catalyzed by SpNic, most likely by reversible formation of the thioester from nicotinic acid catalyzed by the enzyme.

Mutations of Cys136, Lys 103, and Arg97. To further investigate the catalytic mechanism of ^{18}O exchange and of nicotinamidase catalysis, we prepared several active site mutants of SpNic. These were C136A, C136S, K103A, and R97A. The structure of the C136S mutant has been determined by X-ray crystallography, and nicotinamide cocrystallizes in the active site (*35*). We found that C136A and C136S were unable to catalyze nicotinamide hydrolysis down to 10^{-6} s^{-1} sensitivity, consistent with prior work (*35*). These two mutants were unable to catalyze the exchange of ^{18}O into nicotinic acid. The K103A and R97A mutants were prepared on the basis of the prediction that K103A is an active site Lys, which was recently confirmed by crystallography (*35*). R97A is a mutant that our sequence predictions indicate is possibly in the active site (Figure 1) but was shown by crystallography to be far from the catalytic site (*35*). Consistently, we found that the R97A mutant was a robust nicotinamidase and was nearly as good as the native enzyme in promoting ^{18}O exchange. The K103A mutant had only 2.2% of the catalytic activity of the native enzyme in the ^{18}O exchange reaction and 0.15% of the native rate in the nicotinamidase reaction (Table 3). This mutant is expressed well, and the slow rate is attributed to the essentiality of this universally conserved lysine in catalysis.

Inhibition by Nicotinaldehyde. A report that *Sa. cerevisiae* nicotinamidase could be weakly inhibited by nicotinaldehyde [K_i = 68 μM (*52*)] led us to wonder if nicotinaldehydes might be general inhibitors of nicotinamidases. Yan et al. (*52*) suggested that nicotinaldehyde inhibited the yeast enzyme by a noncompetitive mechanism via Schiff base formation. We reinvestigated this inhibition and showed that nicotinaldehyde **16** potently inhibits nicotinamidases from all sources we examined (Table 4). Double-reciprocal plots confirmed competitive inhibition with nicotinamide in all cases, in contrast to the report of Yan (*52*). [Three examples are provided in Figure 5 (SpNic, PfNic, and BbNic); other examples are available in the Supporting Information.] Table 4 shows that the determined K_i values were 1.4 μM for the yeast enzyme and 34, 11, and 110 nM for the corresponding enzymes from *Pl. falciparum*, *S. pneumoniae*, and

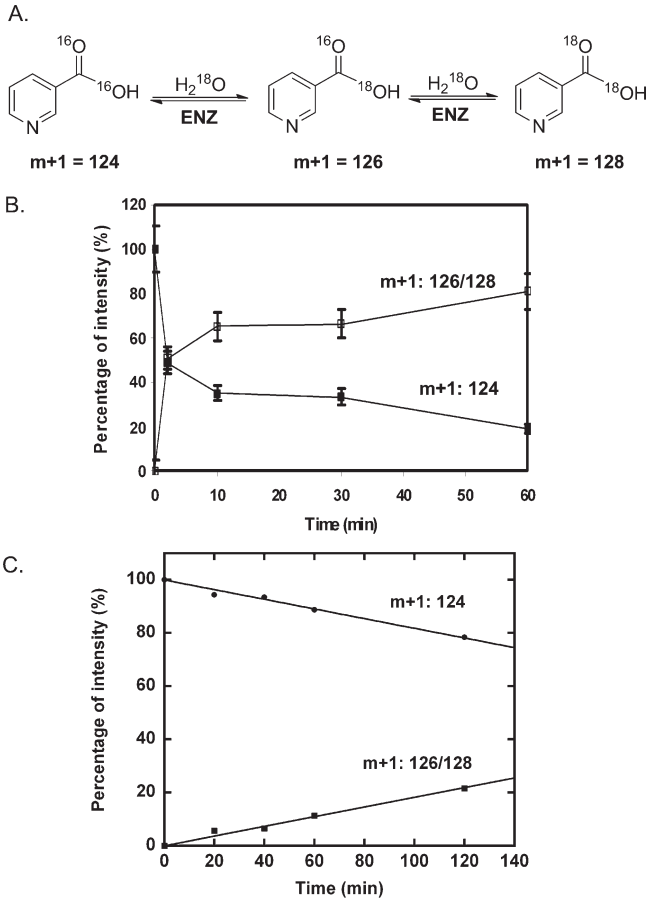

FIGURE 4: Mass spectra demonstrating time-dependent exchange of ^{18}O into nicotinic acid (NA) catalyzed by SpNic. Data are plotted as the percent intensity vs time, where the total intensities of peaks in mass spectra at *m*/*z* 124, 126, and 128 are summed to reach 100%. *m*/*z* 124 is the mass of unlabeled nicotinic acid as a twice protonated cation (M^+); *m*/*z* 126 is the molecular mass of nicotinic acid incorporating a single ^{18}O label, and *m*/*z* 128 is the mass of nicotinic acid incorporating two ^{18}O atoms. Mass intensities of singly and doubly labeled nicotinic acid are summed. The data in panel B show that the mass spectrum of nicotinic acid treated with SpNic in the presence of ^{18}O becomes rapidly depleted of intensity for the peak corresponding to the ion at *m*/*z* 124, whereas there is a corresponding enrichment of *m*/*z* 126 and 128 peak intensities, demonstrating the incorporation of ^{18}O into nicotinic acid. Control does not exchange. (A) Schematic exchange reaction catalyzed by SpNic. (B) Time course of ^{18}O exchange catalyzed by SpNic. The reaction was conducted in 1 mM NA, $H_2{}^{18}O$, and 6 μM SpNic at 37 °C for the indicated time. (C) Determination of the initial rate of ^{18}O exchange. The reaction was conducted in 1 mM NA, $H_2{}^{18}O$, and 100 nM SpNic at 37 °C for the indicated time. The initial rate was determined to be 0.34 s^{-1} after correction for the mole fraction of ^{18}O present in the reaction (eq 4, Materials and Methods).

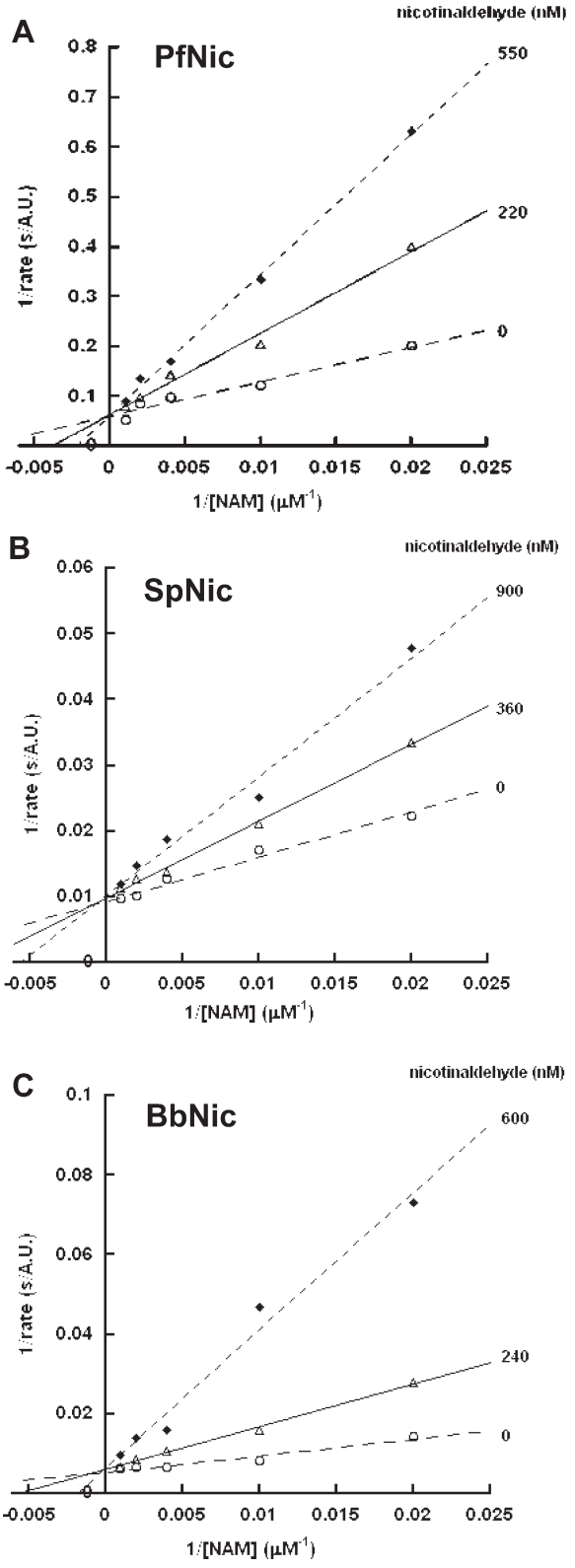

FIGURE 5: Lineweaver–Burke plots for nicotinamidases from *Pl. falciparum* (A), *S. pneumoniae* (B), and *B. burgdorferi* (C) in the presence of nicotinaldehyde determined with a fluorescence plate reader assay. Curves were obtained in the presence of three different concentrations of nicotinaldehyde, demonstrating the competitive nature of the inhibitor with substrate. The units on the *y*-axis are seconds per arbitrary unit. A control showing that nicotinaldehyde does not interfere with the GDH enzyme activity is provided in the Supporting Information.

B. burgdorferi, respectively. Nicotinaldehyde competitively inhibited both *C. elegans* enzymes with K_i values of 22 and 110 nM

Table 3: Nicotinamidase and ^{18}O Exchange Activity of SpNic and Its Mutants

SpNic	catalytic rate[a] [k_{obs} (s^{-1})]	^{18}O exchange rate[d] [k_{obs} (s^{-1})]
wt	3.4[b]	0.34
R97A	3.2[b]	0.27
K103A	0.0053[c]	0.0076
C136A	$< 10^{-6}$[c]	$< 10^{-6}$
C136S	$< 10^{-6}$[c]	ND[e]

[a]The observed rate of nicotinamidase catalysis of SpNic and mutants measured using 200 μM NAM at 37 °C. [b]The rates were determined with a GDH plate reader assay. [c]The rates were determined with a HPLC assay. The full experimental procedure is available in Materials and Methods. [d]The observed exchange of ^{18}O into nicotinic acid catalyzed by SpNic and mutants as measured by the initial rate method and mass spectrometry (Figure 4) in the presence of 1 mM nicotinic acid and $H_2{}^{18}O$ at 37 °C. Enzyme concentrations were 100 nM for SpNic wt and R97A and 5 μM for K103A or C136A. The measured rate was corrected by the mole fraction of ^{18}O in the reaction as described by eq 4 in Materials and Methods. The full experimental procedure is given in Materials and Methods. [e]Not determined.

determined for CePNC2 and CePNC1, respectively (Table 4 and Supporting Information).

Nicotinaldehydes as Inhibitors of Nicotinamidases. To more completely explore the potency of nicotinaldehydes as inhibitors of nicotinamidases, we synthesized a number of substituted analogues of nicotinaldehyde, with variable substituents (as shown in Table 4). The K_i values for inhibition of nicotinamidases are listed in Table 4. Consistent with observations that 5-substituted nicotinamides are excellent substrates, 5-substituted nicotinaldehyde analogues **17**–**19** were potent inhibitors of all of the nicotinamidases tested (Table 4). Several representative curves demonstrating inhibition of nicotinamidases by 5-*O*-methyl- and 5-methylnicotinaldehydes **18** and **19**, respectively, are shown in Figure 6. All enzymes tolerated even a bulky 5-bromo substituent [**17** (Table 4)].

Consistent with observations that 4-*O*-methyl substitution was poorly tolerated in substrates, 4-*O*-methylnicotinaldehyde **22** was a weak inhibitor with a higher K_i value (Table 4). However, **22** was a fair inhibitor of the CePNC2 enzyme, with a 19-fold selectivity over CePNC1, suggesting that variations in chemical structure of these compounds can lead to modest inhibitor selectivity (Table 4). We also tested several other compounds for inhibitory activity, including acetylpyridine **24**, 3-cyanopyridine **23**, 3-hydroxypyridine **25**, and nicotinic acid (Table 4).

DISCUSSION

Mechanism of Inhibition. We propose that the mechanism of aldehyde inhibition parallels the mechanism of catalysis. Nicotinamide initially coordinates the central metal atom and is attacked by the universally conserved active site Cys to form a tetrahedral adduct that subsequently decomposes by elimination of ammonia to yield an enzyme-stabilized thioester. Subsequent hydrolysis of the thioester completes nicotinic acid formation on the enzyme. This overall general mechanistic proposal was first proposed by Fyfe et al. (*34*). We propose that nicotinaldehydes bind the enzyme analogously via coordination of the pyridine N1 atom (Scheme 4). The subsequent attack of the cysteine on the aldehyde occurs in a manner analogous to that envisioned for the substrate, except that instead of forming an unstable intermediate that can decompose to a thioester, the tetrahedral adduct, a thiohemiacetal, is unable to decompose forward and is stalled by

Table 4: K_i Values (micromolar) of Nicotinamidase Inhibitors

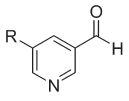

16: R = H
17: R = Br
18: R = OMe
19: R = Me

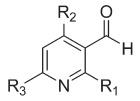

20: R_1 = Cl, R_2, R_3 = H
21: R_1, R_2 = H, R_3 = F
22: R_1, R_3 = H, R_2 = OMe

23: R = CN
24: R = Ac
25: R = OH
nicotinic acid: R = COOH

substrate	BbNic[a]	PfNic[b]	Pnc1[c]	SpNic[d]	CePNC1[e]	CePNC2[f]
16[g]	0.11 ± 0.02	0.034 ± 0.007	1.4 ± 0.1	0.011 ± 0.001	0.11 ± 0.01	0.022 ± 0.004
17[g]	1.3 ± 0.20	0.59 ± 0.14	4.0 ± 0.80	0.071 ± 0.022	0.14 ± 0.02	0.088 ± 0.02
18[g]	0.85 ± 0.04	0.039 ± 0.004	3.8 ± 0.54	0.14 ± 0.02	0.31 ± 0.05	0.14 ± 0.02
19[g]	0.19 ± 0.03	0.023 ± 0.005	0.65 ± 0.07	0.056 ± 0.002	ND[h]	ND[h]
20	370[i]	NI[j]	5000[i]	110[i]	ND[h]	ND[h]
21	18[i]	4.9[i]	NI[j]	0.73 ± 0.29[g]	ND[h]	ND[h]
22	153[i]	1.0 ± 0.11	68[i]	50[i]	5.3 ± 1.0[g]	0.44 ± 0.022[g]
23	2000[i]	1000[i]	85[i]	500[i]	ND[h]	ND[h]
24	342[i]	10[i]	46[i]	60[i]	ND[h]	ND[h]
25	NI[j]	NI[j]	NI[j]	NI[j]	ND[h]	ND[h]
nicotinic acid	NI[j]	NI[j]	NI[j]	2000[i]	NI[j]	NI[j]

[a]Typically 140 nM BbNic. [b]Typically 14 nM PfNic. [c]Typically 210 nM Pnc1. [d]Typically 12 nM SpNic. [e]Typically 10 nM CePNC1. [f]Typically 133 nM CePNC2. In most cases, the inhibitions were determined by the GDH assay as described in Materials and Methods. [g]The inhibition data were fit to Morrison's equation (eq 2) described in Materials and Methods (see examples of data and fits in Figure 6 and in the Supporting Information). The determined K_i^{app} values were converted to the K_i values (the intrinsic binding constant of the inhibitor for the enzyme) listed in Table 4 by eq 3 in Materials and Methods. [h]Not determined. [i]The inhibition data were fit to eq 1 as described in Materials and Methods. [j]No inhibition detected.

enzymatic features that stabilize its tetrahedral geometry, which is the oxyanion hole identified as being Ala155 and Cys159 on the *A. baumanii* enzyme (*34*). Sequence comparisons show that the Ala is highly conserved across nicotinamidases, although it is found to be a Leu131 in the SpNic enzyme, and it has been confirmed by X-ray crystallography that this Leu contributes to the oxyanion hole [Figure 1 and Scheme 4 (*35*)]. The Cys residue is universally conserved, and the $n, n + 4$ relationship in sequence is also conserved across nicotinamidases (Figure 1). The ability of aldehydes to trap Cys nucleophiles of amidases is known, and very potent aldehyde inhibitors that target the caspase enzymes have been synthesized, wherein thiohemiacetal adducts have been demonstrated by X-ray crystallography (*54*). The thiohemiacetal adducts to caspases are stabilized by binding to the oxyanion hole.

The tetrahedral adduct formed can decompose only by reversal of the reaction to the initial aldehyde−metal complex (Scheme 4). We propose that thiohemiacetal adducts form reversibly with solution nicotinaldehyde because the inhibitions observed are competitive with nicotinamide present (Figure 5) and no biphasic onset is apparent for reaction progress curves, and preincubation does not change inhibitor potency (data not shown). K_i values for nicotinaldehyde are smaller than the K_m for nicotinamide by a factor of 91−3450 across all enzymes studied (with the exception of yeast Pnc1, for which $K_m/K_i = 7.6$). The inhibition data are consistent with oxyanion stabilization of the tetrahedral intermediate formed during catalysis, an energy of binding that can also be captured in the form of enzyme-stabilized thioacetal adducts. This mechanism of inhibition was recently confirmed on the SpNic enzyme for nicotinaldehyde **16** and 5-*O*-methylnicotinaldehyde **18** (*35*). We depict the inhibition as depending upon the initial coordination of the aldehyde to the metal center, characterized by a binding constant K_d, which is further stabilized by a factor $1/K_{int}$, where K_{int} is the equilibrium constant for the cysteine adduct versus the Michaelis complex. The inhibition constant can thus be deduced to be $K_i = K_d(K_{int})^{-1}$. This is also qualitatively visualized in the reaction coordinate presented in Scheme 4.

^{18}O Exchange Mechanism and Catalytic Mechanism of Nicotinamidases. The X-ray crystal structure of nicotinic acid coordinated to the nicotinamidase from *A. baumanii* (AbPncA) led to a firm mechanistic proposal for catalysis by Fyfe et al. (*34*). However, we have obtained additional insight into the general properties of these enzymes by determining the substrate specificities, the generality of nicotinaldehyde inhibitions, and the observation that SpNic can catalyze the exchange of ^{18}O into the product nicotinic acid. Mutational studies have also provided new insights. To explain ^{18}O exchange, we propose the mechanism in Scheme 5. Coordination of nicotinic acid to the Zn^{2+}-aqua center places the carboxy of the substrate in the proximity of three universally conserved residues, Asp8, Cys136, and Lys103 (using the SpNic sequence information). Crystallographic data suggest that the conserved Asp can interact equally with the Cys thiol as well as the nicotinate oxygen (*34*, *35*), and this structural arrangement is likely preserved for the corresponding SpNic residue Asp8. We propose that when the universally conserved Asp and the metal-coordinated nicotinic acid share a hydrogen bond, with the Cys nucleophile in thiolate form (SpNic sequence), the nicotinic acid can react by Cys thiolate nucleophilic addition to form a tetrahedral adduct. In this process, full transfer of a proton from Asp occurs. The sp^3 center generated on the substrate bears a hydroxyl substituent, an oxyanion substituent (which is proposed to sit in the oxyanion hole), and a thioether substituent (from nucleophilic Cys). Subsequent tetrahedral intermediate collapse eliminates hydroxide to form a thioester intermediate.

Full expulsion of the hydroxide group from the tetrahedral center would be thermodynamically challenging but could be facilitated by protonation of the leaving group oxygen by Lys103 (SpNic), which is universally conserved in all nicotinamidases and when mutated in *M. tuberculosis* PncA produces an inactive

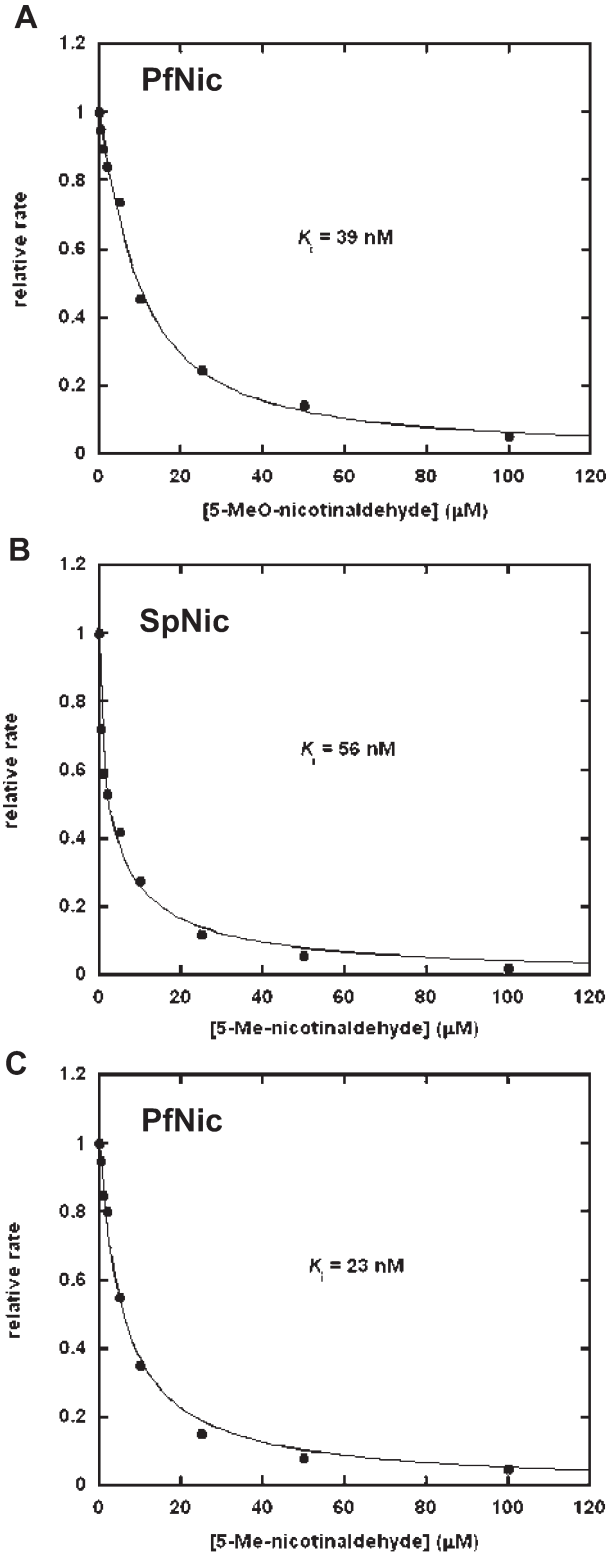

FIGURE 6: Curves showing the inhibition of the nicotinamidase enzymes by 5-*O*-methylnicotinaldehyde [(A) 14 nM PfNic] and 5-methylnicotinaldehyde [(B) 12 nM SpNic and (C) 14 nM PfNic]. The reactions were conducted in the presence of 1 mM nicotinamide and various concentrations of the inhibitor in 1 mM α-ketoglutarate, 250 μM NADH, and 1.5 units of GDH per 100 μL of reaction volume in 100 mM phosphate buffer (pH 7.3). After initiation by addition of the enzyme, the reactions were monitored by fluorescence, and initial rates of reaction were calculated. The curves show the observed rate with respect to inhibitor concentration. Data points are fit to Morrison's equation (*39*) and the K_i calculated from the K_i^{app} value of Morrison's equation as described in Materials and Methods. Controls showing that nicotinaldehydes do not interfere with the GDH enzyme activity are provided in the Supporting Information.

enzyme (*3*, *4*). Correspondingly, in SpNic the K103A mutant has only 2.2% of the activity of the native enzyme as measured by the observed catalytic rate of ^{18}O exchange (Table 3). There is a 4−5 order of magnitude difference in the predicted pK_a values between water and protonated Lys103 (using the free amino acid pK_a value), making proton transfer to form water thermodynamically downhill (Scheme 5). The deprotonation of this Lys is supported by the fact that the ε-N atom is located 4.8 Å from the carboxy oxygen in the AbPncA structure (*34*) and located only 4.70 Å from the carbonyl carbon in the thioester complex in the SpNic thioester structure determined recently (*35*), suggesting there is intervening space for a water to be accommodated. The first half of the exchange reaction is summarized as follows. A thiolate (pK_a = 7−8) is reacted to form a Lys (ε-NH_2, pK_a = 9−10; the free amino acid) with a CysS−C(carbonyl) bond formed and a O−C(carboxy) bond in nicotinic acid cleaved. In addition, two strong O−H bonds are formed in the process of generating water at the active site from deprotonation of two acidic groups (AspCOOH and LysNH_3^+). The overall driving force appears to be formation of water in the active site, making it easier to understand how the barrier to isotope exchange is not significant, as measured by the 0.34 s^{-1} rate constant for this process. The expulsion of water from the thioester site followed by water rebinding (water exchange) permits the leakage of ^{18}O into the active site, and the reaction run in reverse completes a single ^{18}O exchange into the nicotinic acid substrate. Full exchange occurs after many enzymatic turnovers. The flexibility of the SpNic active site appears to be supported by its ability to hydrolyze even the very bulky phenylnicotinate ester (Table 2).

This mechanistic proposal can be applied to understand the total reaction mechanism and suggests an important role for the conserved Lys in the catalytic mechanism that hydrolyzes nicotinamide, supported by our finding that the SpNic K103A mutant loses more than 99% of its catalytic activity in this reaction (Table 3). The proposed overall mechanism is shown in Scheme 6. Initially, nicotinamide coordinates the active site Zn^{2+} complex to form the Michaelis complex. This coordination is proposed to activate the substrate, not only by organizing it into a geometry ideal for catalysis but also by electrophilic activation caused by the Lewis acidity of the Zn^{2+}. The universally conserved Asp deprotonates Cys to form a nucleophilic thiolate that can readily proceed to the tetrahedral intermediate. The transfer of a proton to the amino group of the tetrahedral intermediate facilitates oxyanion electron flow to form the thioester. This mechanism is entirely consistent with the mechanism initially proposed by Fyfe et al. (*34*). However, the ammonia product is quite basic, and with no other protons in the vicinity (except for an aqua-Zn^{2+}), it can deprotonate the active site Lys to form a free amine (ε-NH_2) species prior to its departure from the active site as ammonium. X-ray studies of SpNic suggest that the amide N atom of the substrate is in the proximity of the Lys ε-amino group, with a determined distance of 5.2 Å in the nicotinamide C136S mutant structure (*35*). At this point, our mechanism differs from the mechanism of Fyfe et al., which proposed no active catalytic role for the conserved Lys, except for structural and possibly electrostatic (*34*). The mechanism of Fyfe et al. also proposes that ammonia departs the active site as NH_3, leaving Lys114 of AbPncA unperturbed (*34*).

Our proposed mechanism provides a thermodynamic driving force for hydroxide formation at the active site via the availability of the basic Lys(ε-NH_2). Deprotonation of water by this base is predicted to be uphill with a ΔpK_a of 4−5 (based on the pK_a value

Scheme 4: Mechanism for Nicotinaldehyde Inhibition of Nicotinamidase Enzymes[a]

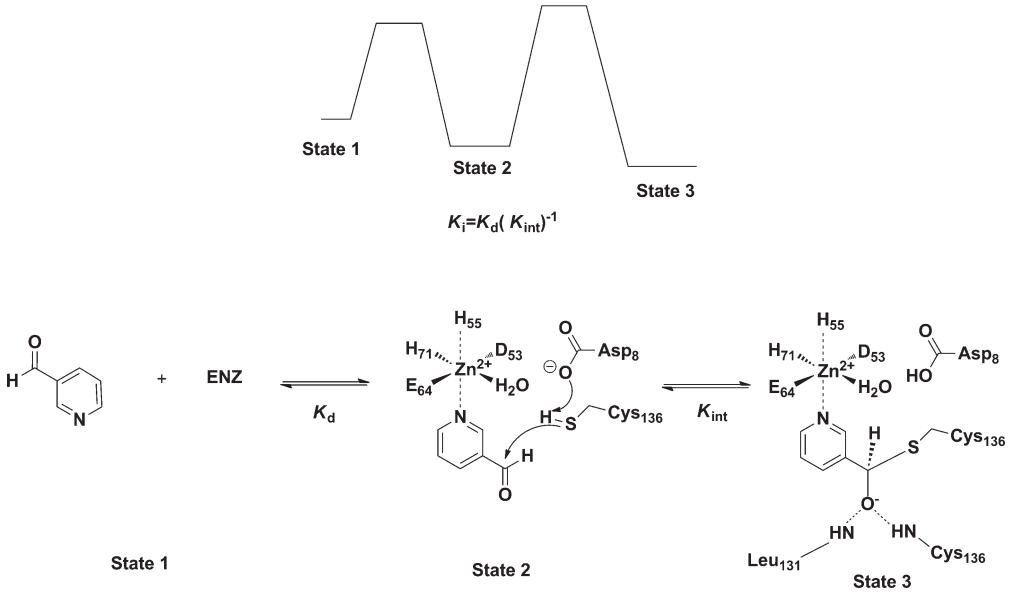

[a]The numbering is from the enzyme from SpNic. The top panel represents a reaction coordinate diagram, where plateaus levels are meant to indicate relative energy.

Scheme 5: Mechanism for the Reversal of Nicotinic Acid to the Nicotinoyl Thioester Complex[a]

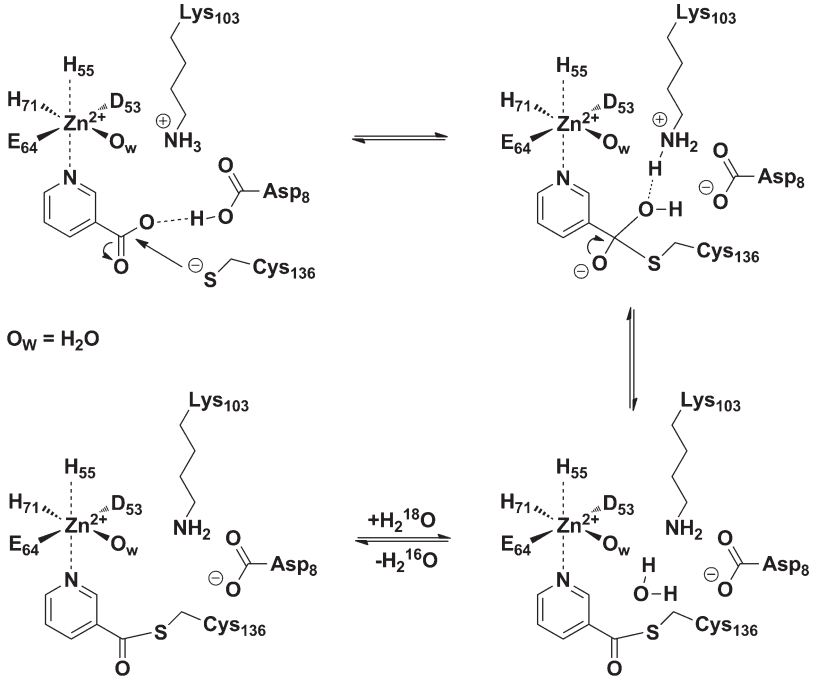

[a]The mechanism explains the ability of SpNic to catalyze the exchange of ^{18}O into nicotinic acid. A key feature of the proposed mechanism is the deprotonation of Lys103 upon thioester formation from nicotinic acid, which then serves as a base catalyst to activate water in the ^{18}O exchange reaction. The numbering system used is for the SpNic enzyme.

of the isolated amino acid). However, additional driving force for deprotonation of water can be obtained by the formation of a salt bridge between the strictly conserved Lys and the strictly conserved Asp located at 2.66 Å in the AbPncA structure (*34*) and also present in the recent SpNic structure (*35*). Hydroxide can then hydrolyze the thioester and complete the catalytic mechanism (Scheme 6). Interestingly, the products formed from nicotinamide to form the thioester exactly reproduce the intermediate and protonation states of active site groups that we invoked to explain the ^{18}O exchange reaction (Scheme 5). As compared with the mechanism of Fyfe et al. (*34*), we do not propose to deprotonate water with an Asp residue, but rather by the Lys amino group, which makes the thermodynamic barrier for hydroxide generation more favorable ($\Delta pK_a \sim 9$ and 4−5, respectively). Our proposed reaction mechanism (Scheme 6) is completed in analogy to the proposed mechanism for ^{18}O exchange (Scheme 5). An additional advantage of our mechanism is that it does not require generation of a protonated and Zn^{2+}-coordinated nicotinic acid at the active site as proposed by Fyfe et al. (*34*). Nicotinic acid acidity is characterized by a pK_a near 3, and the

Scheme 6: Proposed Mechanism of Nicotinamidases[a]

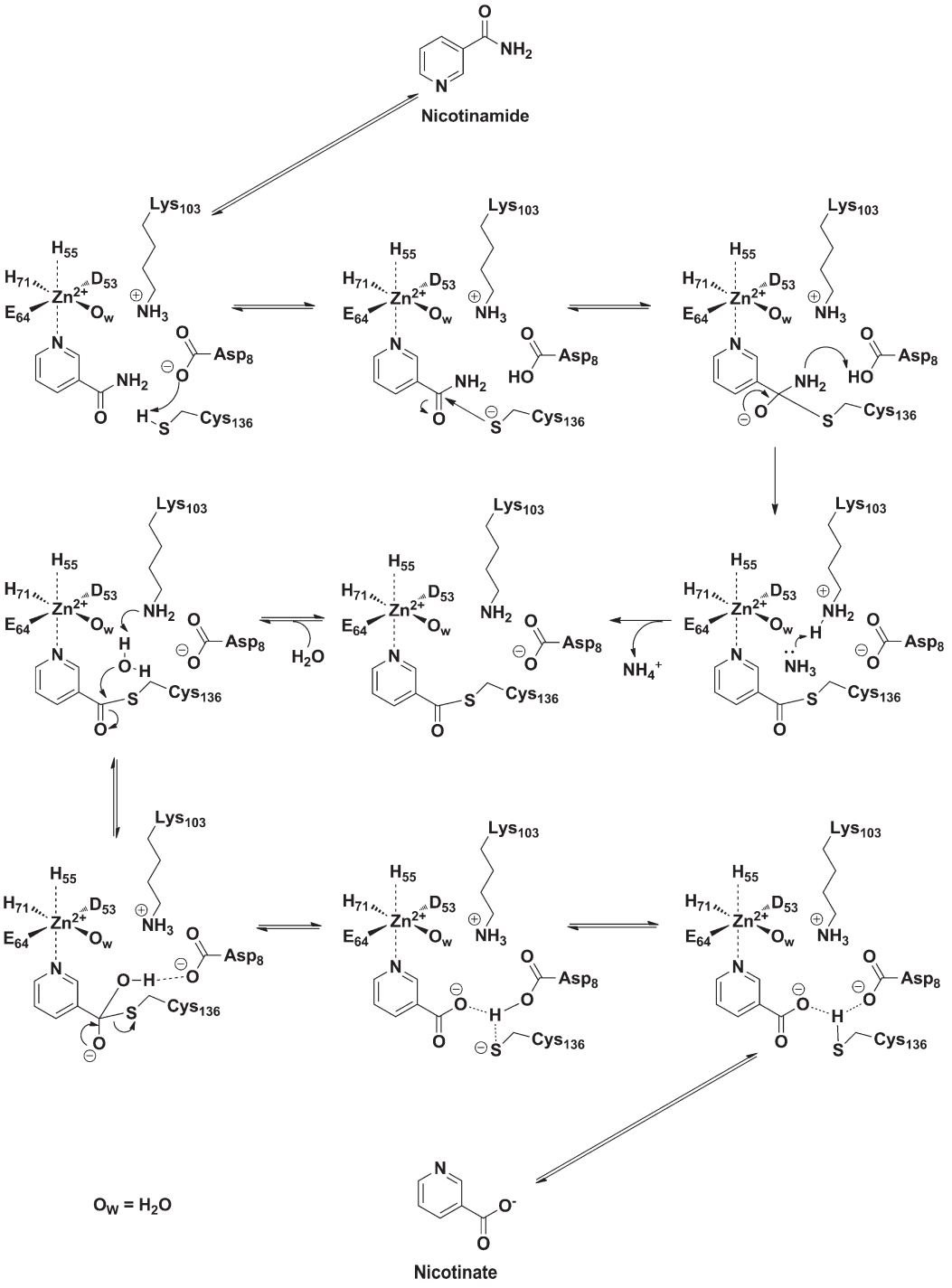

[a]The ammonia generated in the first half of the reaction coordinate generates a deprotonated Lys residue prior to departure from the active site. The intermediacy of this Lys is envisioned to act as a base catalyst that activates a water to complete the second half of the catalytic reaction. The numbering system is that for the SpNic enzyme.

coordination to an acidifying Zn^{2+} center would make this protonation thermodynamically unfavorable.

Other mechanistic alternatives could be imagined. For example, the role we propose for the Lys could be played by the aqua-Zn^{2+}. Aqua-Zn^{2+} coordination sites proximal to the substrate carbonyl position have been identified for all four crystallographically determined nicotinamidases, Pnc1 (*6*), AbPncA (*34*), *P. horikoshii* PncA (*33*), and most recently the full set of SpNic structures (*35*). In the SpNic thioester structure, the coordinated water oxygen is located 5.5 Å from the thioester carboxy oxygen (*35*). A mechanistic scheme that invokes this role for the proximal aqua-Zn^{2+} is shown in Scheme 7. Inspection of the X-ray structure of AbPncA indicates that the aqua-Zn^{2+} center probably is too far from the active site position where protonations and deprotonations are required, but strictly speaking we cannot rule out this possibility. An aqua-Zn^{2+} species typically has a pK_a of 7−8 (*55*), which could provide an effective quench for active site-generated ammonia, and the resulting Zn−OH species would have a more favorable pK_a trade-off (~6−7) than Asp (9) for generating hydroxide within the active site. There is

Scheme 7: Alternative Aqua-Zn^{2+} Mechanism of Nicotinamidases[a]

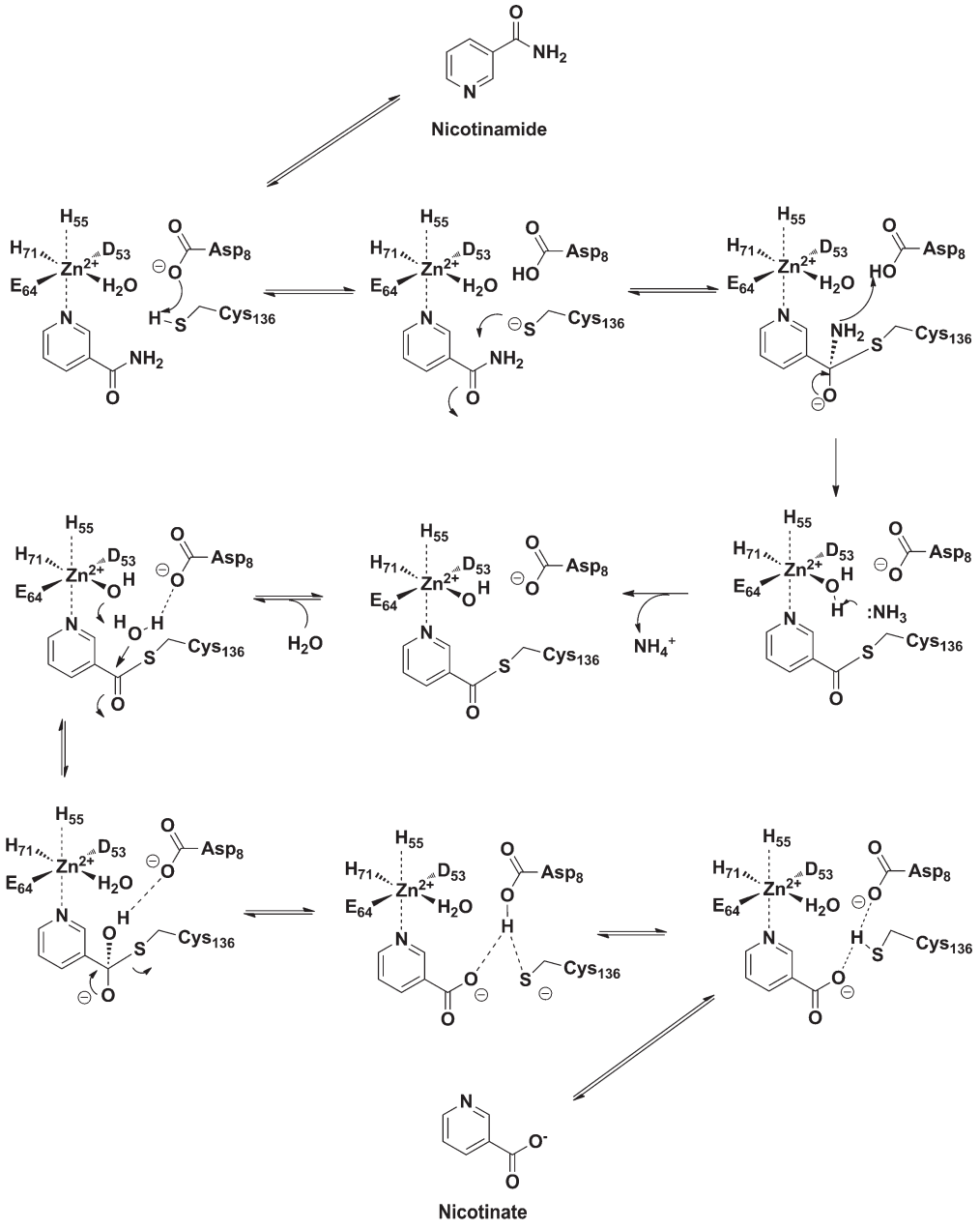

[a]The ammonia generated in the first half of the reaction coordinate generates a Zn-hydroxide by deprotonation prior to departure from the active site. The intermediacy of a Zn-hydroxide is envisioned to act as a base catalyst that activates a solvent-derived nucleophilic water in the second half of the catalytic reaction. The numbering system used is for the SpNic enzyme.

also the possibility that both aqua-Zn^{2+} and the conserved Lys provide duplication of function within the active site, because ammonia formed from substrate is small and can be expected to leak out of the enzyme rapidly. We propose that ammonia protonation in the active site drives the reaction forward to thioester formation, likely prevents reverse commitment, and prepares the active site for hydroxide generation. To guarantee that this occurs, two potential routes for ammonia quenches in the active site may have coevolved. Theoretically, the conjugate bases formed by quench of ammonia (Lys103-NH_2, or Zn-OH) are basic enough to activate water to complete catalysis. Further experimental studies are required to sort out these possibilities and to decide which mechanism is most likely for distinct nicotinamidase enzymes.

The generality of nicotinaldehyde inhibition across broad phylogenetic sources of nicotinamidases, conservation of key catalytic residues (Asp, Cys, and Lys), and the requirement of an active site metal ion indicate that, as a class, nicotinamidases are likely to have similar catalytic mechanisms for accomplishing nicotinamide hydrolysis chemistry. Inhibitors of nicotinamidases are expected to be useful for investigating the diverse functions of these enzymes in a multitude of biological settings. Investigations of nicotinamidase inhibitors as antimicrobials are also clearly of interest.

ACKNOWLEDGMENT

We thank Dr. Haiteng Deng of the Proteomics Resource of Rockefeller University for assistance with obtaining MALDI-MS data. We also thank the Mass Spectrum Facility of Hunter College for HRMS data.

SUPPORTING INFORMATION AVAILABLE

Methods of cloning and expression of enzymes, mutant construction, HPLC demonstration of catalytic activity of nicotinamidases, inhibitions of nicotinamidases, demonstration by NMR of PfNic-catalyzed hydrolysis of phenylnicotinate, and metal ion studies. This material is available free of charge via the Internet at http://pubs.acs.org.

REFERENCES

1. Gerdes, S. Y., Scholle, M. D., D'Souza, M., Bernal, A., Baev, M. V., Farrell, M., Kurnasov, O. V., Daugherty, M. D., Mseeh, F., Polanuyer, B. M., Campbell, J. W., Anantha, S., Shatalin, K. Y., Chowdhury, S. A., Fonstein, M. Y., and Osterman, A. L. (2002) From genetic footprinting to antimicrobial drug targets: Examples in cofactor biosynthetic pathways. *J. Bacteriol. 184*, 4555–4572.
2. Boshoff, H. I., and Mizrahi, V. (1998) Purification, gene cloning, targeted knockout, overexpression, and biochemical characterization of the major pyrazinamidase from *Mycobacterium smegmatis*. *J. Bacteriol. 180*, 5809–5814.
3. Zhang, H., Deng, J. Y., Bi, L. J., Zhou, Y. F., Zhang, Z. P., Zhang, C. G., Zhang, Y., and Zhang, X. E. (2008) Characterization of *Mycobacterium tuberculosis* nicotinamidase/pyrazinamidase. *FEBS J. 275*, 753–762.
4. Scorpio, A., and Zhang, Y. (1996) Mutations in pncA, a gene encoding pyrazinamidase/nicotinamidase, cause resistance to the antituberculous drug pyrazinamide in tubercle bacillus. *Nat. Med. 2*, 662–667.
5. Ghislain, M., Talla, E., and Francois, J. M. (2002) Identification and functional analysis of the *Saccharomyces cerevisiae* nicotinamidase gene, PNC1. *Yeast 19*, 215–224.
6. Hu, G., Taylor, A. B., McAlister-Henn, L., and Hart, P. J. (2007) Crystal structure of the yeast nicotinamidase Pnc1p. *Arch. Biochem. Biophys. 461*, 66–75.
7. Joshi, J. G., and Handler, P. (1962) Purification and properties of nicotinamidase from *Torula cremoris*. *J. Biol. Chem. 237*, 929–935.
8. Zerez, C. R., Roth, E. F., Jr., Schulman, S., and Tanaka, K. R. (1990) Increased nicotinamide adenine dinucleotide content and synthesis in *Plasmodium falciparum*-infected human erythrocytes. *Blood 75*, 1705–1710.
9. Wang, G., and Pichersky, E. (2007) Nicotinamidase participates in the salvage pathway of NAD biosynthesis in *Arabidopsis*. *Plant J. 49*, 1020–1029.
10. Balan, V., Miller, G. S., Kaplun, L., Balan, K., Chong, Z. Z., Li, F., Kaplun, A., VanBerkum, M. F., Arking, R., Freeman, D. C., Maiese, K., and Tzivion, G. (2008) Life span extension and neuronal cell protection by *Drosophila* nicotinamidase. *J. Biol. Chem. 283*, 27810–27819.
11. van der Horst, A., Schavemaker, J. M., Pellis-van Berkel, W., and Burgering, B. M. (2007) The *Caenorhabditis elegans* nicotinamidase PNC-1 enhances survival. *Mech. Ageing Dev. 128*, 346–349.
12. Vrablik, T. L., Huang, L., Lange, S. E., and Hanna-Rose, W. (2009) Nicotinamidase modulation of NAD^+ biosynthesis and nicotinamide levels separately affect reproductive development and cell survival in *C. elegans*. *Development 136*, 3637–3646.
13. Oppenheimer, N. J. (1994) NAD Hydrolysis: Chemical and Enzymatic Mechanisms. *Mol. Cell. Biochem. 138*, 245–251.
14. Handlon, A. L., Xu, C., Mullersteffner, H. M., Schuber, F., and Oppenheimer, N. J. (1994) 2′-Ribose Substituent Effects on the Chemical and Enzymatic-Hydrolysis of NAD^+. *J. Am. Chem. Soc. 116*, 12087–12088.
15. Johnson, R. W., Marschner, T. M., and Oppenheimer, N. J. (1988) Pyridine-Nucleotide Chemistry: A New Mechanism for the Hydroxide-Catalyzed Hydrolysis of the Nicotinamide Glycosyl Bond. *J. Am. Chem. Soc. 110*, 2257–2263.
16. Sauve, A. A., Wolberger, C., Schramm, V. L., and Boeke, J. D. (2006) The biochemistry of sirtuins. *Annu. Rev. Biochem. 75*, 435–465.
17. Grimm, D., Tilly, K., Bueschel, D. M., Fisher, M. A., Policastro, P. F., Gherardini, F. C., Schwan, T. G., and Rosa, P. A. (2005) Defining plasmids required by *Borrelia burgdorferi* for colonization of tick vector *Ixodes scapularis* (Acari: Ixodidae). *J. Med. Entomol. 42*, 676–684.
18. Kawabata, H., Norris, S. J., and Watanabe, H. (2004) BBE02 disruption mutants of *Borrelia burgdorferi* B31 have a highly transformable, infectious phenotype. *Infect. Immun. 72*, 7147–7154.
19. Purser, J. E., Lawrenz, M. B., Caimano, M. J., Howell, J. K., Radolf, J. D., and Norris, S. J. (2003) A plasmid-encoded nicotinamidase (PncA) is essential for infectivity of *Borrelia burgdorferi* in a mammalian host. *Mol. Microbiol. 48*, 753–764.
20. Kim, S., Kurokawa, D., Watanabe, K., Makino, S., Shirahata, T., and Watarai, M. (2004) *Brucella abortus* nicotinamidase (PncA) contributes to its intracellular replication and infectivity in mice. *FEMS Microbiol. Lett. 234*, 289–295.
21. Sauve, A. A. (2008) NAD^+ and vitamin B3: From metabolism to therapies. *J. Pharmacol. Exp. Ther. 324*, 883–893.
22. Anderson, R. M., Bitterman, K. J., Wood, J. G., Medvedik, O., and Sinclair, D. A. (2003) Nicotinamide and PNC1 govern lifespan extension by calorie restriction in *Saccharomyces cerevisiae*. *Nature 423*, 181–185.
23. Bitterman, K. J., Anderson, R. M., Cohen, H. Y., Latorre-Esteves, M., and Sinclair, D. A. (2002) Inhibition of silencing and accelerated aging by nicotinamide, a putative negative regulator of yeast sir2 and human SIRT1. *J. Biol. Chem. 277*, 45099–45107.
24. Gallo, C. M., Smith, D. L., Jr., and Smith, J. S. (2004) Nicotinamide clearance by Pnc1 directly regulates Sir2-mediated silencing and longevity. *Mol. Cell. Biol. 24*, 1301–1312.
25. Rogina, B., and Helfand, S. L. (2004) Sir2 mediates longevity in the fly through a pathway related to calorie restriction. *Proc. Natl. Acad. Sci. U.S.A. 101*, 15998–16003.
26. Wood, J. G., Rogina, B., Lavu, S., Howitz, K., Helfand, S. L., Tatar, M., and Sinclair, D. (2004) Sirtuin activators mimic caloric restriction and delay ageing in metazoans. *Nature 430*, 686–689.
27. Tissenbaum, H. A., and Guarente, L. (2001) Increased dosage of a sir-2 gene extends lifespan in *Caenorhabditis elegans*. *Nature 410*, 227–230.
28. Berdichevsky, A., Viswanathan, M., Horvitz, H. R., and Guarente, L. (2006) *C. elegans* SIR-2.1 interacts with 14-3-3 proteins to activate DAF-16 and extend life span. *Cell 125*, 1165–1177.
29. Kaeberlein, M., McVey, M., and Guarente, L. (1999) The SIR2/3/4 complex and SIR2 alone promote longevity in *Saccharomyces cerevisiae* by two different mechanisms. *Genes Dev. 13*, 2570–2580.
30. Lin, S. J., Defossez, P. A., and Guarente, L. (2000) Requirement of NAD and SIR2 for life-span extension by calorie restriction in *Saccharomyces cerevisiae*. *Science 289*, 2126–2128.
31. Hunt, L., Holdsworth, M. J., and Gray, J. E. (2007) Nicotinamidase activity is important for germination. *Plant J. 51*, 341–351.
32. Hughes, D. E., and Williamson, D. H. (1952) The synthesis of cozymase from nicotinic acid and its derivatives by *Lactobacillus arabinosus* 17-5. *Biochem. J. 51*, 330–338.
33. Du, X., Wang, W., Kim, R., Yakota, H., Nguyen, H., and Kim, S. H. (2001) Crystal structure and mechanism of catalysis of a pyrazinamidase from *Pyrococcus horikoshii*. *Biochemistry 40*, 14166–14172.
34. Fyfe, P. K., Rao, V. A., Zemla, A., Cameron, S., and Hunter, W. N. (2009) Specificity and mechanism of *Acinetobacter baumanii* nicotinamidase: Implications for activation of the front-line tuberculosis drug pyrazinamide. *Angew. Chem., Int. Ed. 48*, 9176–9179.
35. French, J. B., Cen, Y., Sauve, A. A., and Ealick, S. E. (2010) High-Resolution Crystal Structures of *Streptococcus pneumoniae* Nicotinamidase with Trapped Intermediates Provide Insights into the Catalytic Mechanism and Inhibition by Aldehydes. *Biochemistry 49*, 8803–8812.
36. Pruser, J. E., Lawrenz, M. B., Caimano, M. J., Howell, J. K., Radolf, J. D., and Norris, S. J. (2003) A plasmid-encoded nicotinamidase (PncA) is essential for infectivity of *Borrelia burgdorferi* in a mammalian host. *Mol. Microbiol. 48*, 753–764.
37. Bradford, M. M. (1976) A rapid and sensitive method for the quantitation of microgram quantities of protein utilizing the principle of protein-dye binding. *Anal. Biochem. 72*, 248–254.
38. Yun, S. L., and Suelter, C. H. (1977) A simple method for calculating Km and V from a single enzyme reaction progress curve. *Biochim. Biophys. Acta 480*, 1–13.
39. Copeland, R. A. (2005) Tight Binding Inhibition. In Evaluation of Enzyme Inhibitors in Drug Discovery, pp 185−192, Wiley-Interscience, Hoboken, NJ.
40. Sauve, A. A., and Schramm, V. L. (2002) Mechanism-based inhibitors of CD38: A mammalian cyclic ADP-ribose synthetase. *Biochemistry 41*, 8455–8463.
41. Evans, G. B., Furneaux, R. H., Gainsford, G. J., Hanson, J. C., Kicska, G. A., Sauve, A. A., Schramm, V. L., and Tyler, P. C. (2003) 8-Aza-immucillins as transition-state analogue inhibitors of purine nucleoside phosphorylase and nucleoside hydrolases. *J. Med. Chem. 46*, 155–q60.
42. Boovanahalli, S. K., Jin, X., Jin, Y., Kim, J. H., Dat, N. T., Hong, Y. S., Lee, J. H., Jung, S. H., Lee, K., and Lee, J. J. (2007) Synthesis of (aryloxyacetylamino)-isonicotinic/nicotinic acid analogues as potent hypoxia-inducible factor (HIF)-1α inhibitors. *Bioorg. Med. Chem. Lett. 17*, 6305–6310.

43. Martin, R. B., and Hull, J. G. (1964) Reactions of N1-Methylnicotinamide Cation + Analogues with Dilute Alkali. *J. Biol. Chem. 239*, 1237–1241.
44. Comins, D. L., and Killpack, M. O. (1990) Lithiation of Methoxypyridines Directed by α-Amino Alkoxides. *J. Org. Chem. 55*, 69–73.
45. Carceller, E., Merlos, M., Giral, M., Balsa, D., Almansa, C., Bartroli, J., Garcia-Rafanell, J., and Forn, J. (1994) [(3-Pyridylalkyl)-piperidylidene]benzocycloheptapyridine derivatives as dual antagonists of PAF and histamine. *J. Med. Chem. 37*, 2697–2703.
46. Bandgar, B. P., Sadavarte, V. S., and Uppalla, L. S. (2000) Selective and rapid oxidation of primary, allylic and benzylic alcohols to the corresponding carbonyl compounds with NaNO2-acetic anhydride under mild and solvent-free conditions. *J. Chem. Soc., Perkin Trans. 1*, 3559–3560.
47. Rife, J. E., and Cleland, W. W. (1980) Kinetic mechanism of glutamate dehydrogenase. *Biochemistry 19*, 2321–2328.
48. Engel, P. C., and Dalziel, K. (1967) The equilibrium constants of the glutamate dehydrogenase systems. *Biochem. J. 105*, 691–695.
49. Smith, B. C., Hallows, W. C., and Denu, J. M. (2009) A continuous microplate assay for sirtuins and nicotinamide-producing enzymes. *Anal. Biochem. 394*, 101–109.
50. Hughes, D. E., and Williamson, D. H. (1953) The deamidation of nicotinamide by bacteria. *Biochem. J. 55*, 851–856.
51. Tanigawa, Y., Shimoyama, M., and Ueda, I. (1980) Nicotinamide deamidase from *Flavobacterium peregrinum*. *Methods Enzymol. 66*, 132–136.
52. Yan, C., and Sloan, D. L. (1987) Purification and characterization of nicotinamide deamidase from yeast. *J. Biol. Chem. 262*, 9082–9087.
53. Calbreath, D. F., and Joshi, J. G. (1971) Inhibition of nicotinamidase by nicotinamide adenine dinucleotide. *J. Biol. Chem. 246*, 4334–4339.
54. Margolin, N., Raybuck, S. A., Wilson, K. P., Chen, W., Fox, T., Gu, Y., and Livingston, D. J. (1997) Substrate and inhibitor specificity of interleukin-1β-converting enzyme and related caspases. *J. Biol. Chem. 272*, 7223–7228.
55. Groves, J. T., and Olson, J. R. (1985) Models of Zinc-Containing Proteases: Rapid Amide Hydrolysis by an Unusually Acidic Zn^{2+}-OH_2 Complex. *Inorg. Chem. 24*, 2715–2717.
56. Chenna, R., Sugawara, H., Koike, T., Lopez, R., Higgins, T. J., Desmond, G., and Thompson, J. D. (2003) Multiple sequence alignment with the Clustal series of programs. *Nucleic Acids Res. 31*, 3497–3500.
57. Gouet, P., Robert, X., and Courcelle, E. (2003) ESPript/ENDscript; extracting and rendering sequence and 3D information from atomic structures of proteins. *Nucleic Acids Res. 31*, 3320–3323.